

## INFORMATION TO USERS

This manuscript has been reproduced from the microfilm master. UMI films the text directly from the original or copy submitted. Thus, some thesis and dissertation copies are in typewriter face, while others may be from any type of computer printer.

**The quality of this reproduction is dependent upon the quality of the copy submitted.** Broken or indistinct print, colored or poor quality illustrations and photographs, print bleedthrough, substandard margins, and improper alignment can adversely affect reproduction.

In the unlikely event that the author did not send UMI a complete manuscript and there are missing pages, these will be noted. Also, if unauthorized copyright material had to be removed, a note will indicate the deletion.

Oversize materials (e.g., maps, drawings, charts) are reproduced by sectioning the original, beginning at the upper left-hand corner and continuing from left to right in equal sections with small overlaps. Each original is also photographed in one exposure and is included in reduced form at the back of the book.

Photographs included in the original manuscript have been reproduced xerographically in this copy. Higher quality 6" x 9" black and white photographic prints are available for any photographs or illustrations appearing in this copy for an additional charge. Contact UMI directly to order.

**UMI<sup>®</sup>**

Bell & Howell Information and Learning  
300 North Zeeb Road, Ann Arbor, MI 48106-1346 USA  
800-521-0600



**University of Alberta**

**A Multi-reflection Cell for Enhanced Absorbance Detection in  
Microchip-based Capillary Electrophoresis Devices**

by

Yutao Jiang



A thesis submitted to the Faculty of Graduate Studies and Research in  
partial fulfillment of the requirements for the degree of Master of Science.

Department of Chemistry

Edmonton, Alberta

Spring 1999



National Library  
of Canada

Bibliothèque nationale  
du Canada

Acquisitions and  
Bibliographic Services

Acquisitions et  
services bibliographiques

395 Wellington Street  
Ottawa ON K1A 0N4  
Canada

395, rue Wellington  
Ottawa ON K1A 0N4  
Canada

*Your file Votre référence*

*Our file Notre référence*

The author has granted a non-exclusive licence allowing the National Library of Canada to reproduce, loan, distribute or sell copies of this thesis in microform, paper or electronic formats.

L'auteur a accordé une licence non exclusive permettant à la Bibliothèque nationale du Canada de reproduire, prêter, distribuer ou vendre des copies de cette thèse sous la forme de microfiche/film, de reproduction sur papier ou sur format électronique.

The author retains ownership of the copyright in this thesis. Neither the thesis nor substantial extracts from it may be printed or otherwise reproduced without the author's permission.

L'auteur conserve la propriété du droit d'auteur qui protège cette thèse. Ni la thèse ni des extraits substantiels de celle-ci ne doivent être imprimés ou autrement reproduits sans son autorisation.

0-612-40064-6

Canada

**University of Alberta**

**Library Release Form**

**Name of Author:** Yutao Jiang

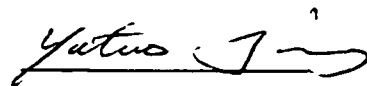
**Title of Thesis:** A Multi-reflection Cell for Enhanced Absorbance  
Detection in Microchip-based Capillary  
Electrophoresis Devices

**Degree :** Master of Science

**Year This Degree Granted:** 1999

Permission is hereby granted to the University of Alberta Library to reproduce single copies of this thesis and to lend or sell such copies for private, scholarly, or scientific research purposes only.

The author reserves all other publication and other rights in association with the copyright in the thesis, and except as herein before provided, neither the thesis nor any substantial portion thereof may be printed or otherwise reproduced in any material form whatsoever without the author's prior written permission.



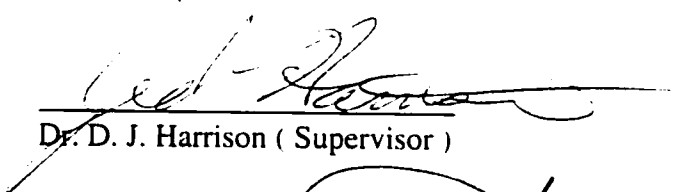
Yutao Jiang  
#305 10812-111 St.  
Edmonton, AB, T5H 3G4

November 20 , 1998

# University of Alberta

## Faculty of Graduate Studies and Research

The Undersigned certify that they have read, and recommend to the Faculty of Graduate Studies and Research for acceptance, a thesis entitled A Multi-reflection Cell for Enhanced Absorbance Detection in Microchip-based Capillary Electrophoresis Devices submitted by Yutao Jiang in partial fulfillment of the requirements for the degree of Master of Science.



Dr. D. J. Harrison ( Supervisor )



Dr. M. McDermott



Dr. AM Robinson

Date Nov 19/98

## **Abstract**

The design, fabrication and testing of a photolithographically fabricated, glass-based multireflection absorbance cell for microfluidic devices, in particular microchip-based capillary electrophoresis (CE) systems is described. A multi-reflection cell was fabricated lithographically using a three mask process to pattern Al mirrors above and below a flow channel in a chip, with 30  $\mu\text{m}$  diam. Optical entrance or exit aperture were positioned 200  $\mu\text{m}$  apart. Light source and detector were positioned on opposite sides, and the metal mirrors were made 1  $\text{cm}^2$  square, to reduce stray light effects. Calibration curves using bromothymol blue (BTB) with a 633 nm light source were linear between 10  $\mu\text{M}$  to 1000  $\mu\text{M}$ . Effective optical pathlengths of 50 to 272  $\mu\text{m}$  were achieved. This device can give much higher absorbance sensitivity and should be much easier to manufacture than planar, glass-based devices previously reported.

# Contents

<b>Chapter One. Introduction</b>	<b>1</b>
1.1 Chip-based Capillary Electrophoresis	1
1.2 Detection Method	4
1.3 Micromachining	4
1.4 Capillary Electrophoresis	6
1.5 Multiple Reflection Absorption Cell	12
1.6 Scope of Present Work	14
References	17
<b>Chapter Two. Theory and Design</b>	<b>20</b>
2.1 Introduction	20
2.2 Beer and Lambert Law	20
2.3 Multi-reflection Cell Considerations	21
2.4 Absorbance Cell Design	26
2.4.1 Mirror and Aperture Design	26
2.4.2 Design 1	26
2.4.3 Design 2	28
2.5 Fabrication Issues	28
References	30
<b>Chapter Three. Glass Bonding Procedures</b>	<b>31</b>
3.1 Introduction	31
3.2 Bonding Considerations of Programfor 0211 Glass	31
3.3 Experiment	32
3.3.1 Material	32
3.3.2 Cleaning	32



3.3.3 Bonding Conditions .....	33
a. Bonding Time Test .....	33
b. Bonding Temperature Test .....	33
c. Other Test .....	34
d. Conclusion .....	34
3.4 Three-Piece Bonding Test .....	35
3.4.1 Introduction .....	35
3.4.2 Bonding Test .....	35
References .....	35

## **Chapter Four. The Choice of Metal for Mirrors ..... 36**

4.1 Introduction .....	36
4.2 The Method for Determining the Absolute Reflectance of Metallic Film .....	38
4.2.1 Theory .....	38
4.2.2 Calculating the Absolute Reflectance .....	40
4.2.3 Experiment .....	42
a. Reflectance Measurements.....	42
b. Transmission Measurement .....	42
4.3 Measurement of Mirror Material .....	44
4.4 The Bonding Effect Test .....	48
4.5 The Effect of Metal Thickness .....	49
4.6 Deposition Method Effect .....	50
4.7 Summary .....	51
References .....	52

## **Chapter Five. Chip Fabrication .....53**

5.1 Introduction .....	53
5.2 The Fabrication of Design 1 .....	53
5.3 The Fabrication of Design 2 .....	54
5.3.1 The Test of Glass Cleaning with Al on it .....	56

5.3.2 Drilling Test on Bonding Glass .....	57
5.3.3 The Fabrication of Design 2 .....	57
5.4 Conclusion and Discussion .....	59
References.....	59
<b>Chapter Six. Measurement, Result and Discussion ..</b>	<b>60</b>
6.1 Introduction .....	60
6.2 Instrumentation .....	60
6.3 Reagents .....	62
6.4 Procedures .....	62
6.5 Light Throughput and Noise .....	62
6.6 Sensitivity .....	63
6.7 Calibration Curve .....	68
6.8 Result and Discussion .....	68
6.9 Conclusion .....	73
References.....	74

## List of Figures

Figure 1.1	The basic structure of chip-based capillary. ....	2
Figure 1.2	The double T injection system. ....	3
Figure 1.3	U-cell detection system. ....	5
Figure 1.4	One mask fabrication process. ....	7
Figure 1.5	General schematic of a conventional CE instrument. ....	9
Figure 1.6	Diagram illustrating the separation of charged and uncharged species in capillary electrophoresis. ....	10
Figure 1.7	Diagram of internal reflection absorbance cell. ....	13
Figure 1.8	Attenuated total reflection infrared absorbance cell. ....	15
Figure 2.1	Multiple reflection absorbance cell on microchip-based capillary. ....	22
Figure 2.2	Relevant dimensions and angle for determining optical path length. ....	23
Figure 2.3	Calculation for multi-reflection cells ....	25
	a ) Plot of the calculated path length as function of the incident beam. ....	
	b ) Plot of the calculated number of reflections versus incident beam angle. ....	
Figure 2.4	Design 1. ....	27
	( a ) Top view of the chip. ....	

( b ) Side view of the chip.

( c ) Top view of the mirror.

Figure 2.5	Design 2. ....	29
Figure 4.1	Spectral reflectance of certain metals. ....	37
Figure 4.2	Transmission measurement system. ....	43
Figure 4.3	Reflectance measurement. ....	45
	a ) Metal-air.	
	b ) Metal-glass.	
Figure 4.4	Thin Cr reflectance measurement of Au. ....	47
Figure 5.1	Fabrication procedure of design 1. ....	55
Figure 5.2	Fabrication procedure of design 2. ....	58
Figure 6.1	The optical instrumentation setup. ....	61
Figure 6.2	The initial mirror test setup to show the multiple reflection cell could work. ....	64
Figure 6.3	Intensity versus incident beam angle of plain Mirror. ....	65
Figure 6.4	Diode photocurrent as a function of incident beam angle. ....	66
Figure 6.5	No offset device.....	67
Figure 6.6	Effective path length as a function of incident beam. ....	69
Figure 6.7	$10^{-5}$ M BTB absorbance peak. ....	70
Figure 6.8	BTB calibration curve of design 2. ....	71

## **List of Tables**

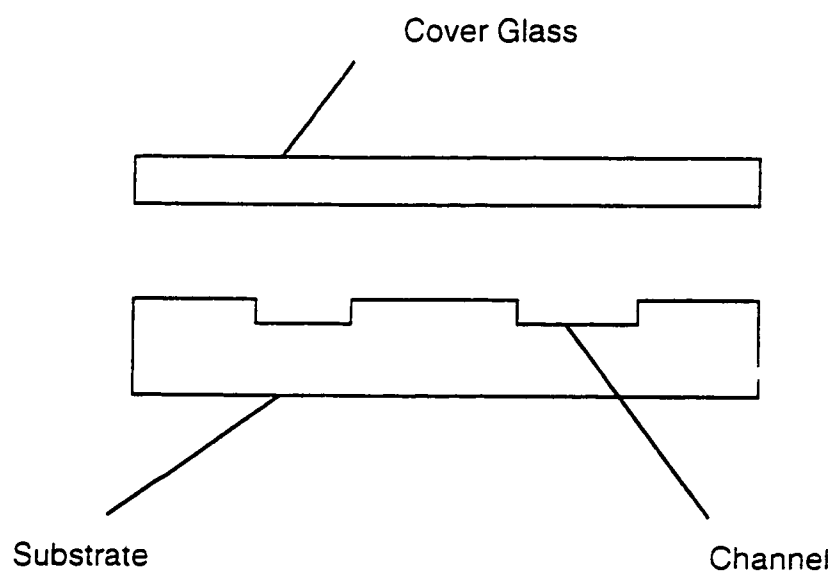
Table 3.1 Previous Bonding condition of mask glass. ....	32
Table 3.2 Bonding condition of 0211 glass. ....	34
Table 4.1 Silicon theoretical reflectance. ....	42
Table 4.2 The reflectivity of some metal films. ....	46
Table 4.3 The reflectivity of 133 Å Cr covered with Au. ....	48
Table 4.4 The effect of bonding on transmission and reflectivity. ....	49
Table 4.5 The effect of thickness of Al film on transmission and reflectivity. ....	50
Table 4.6 Deposition method of Al affect on transmission and. reflectivity. ....	51
Table 5.1 The effect of HNO <sub>3</sub> on transmission and reflectance of Al film. ....	56

# **Chapter One Introduction**

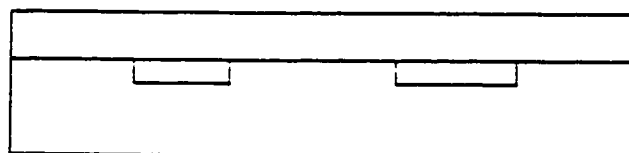
## **1.1 Chip-based Capillary Electrophoresis**

Chip-based capillary electrophoresis is a new technique based on capillary electrophoresis, where small channels are etched on a planar substrate using micromachining technology (1,2,3). Using high voltage as a pump, a sample is separated in the channel as in capillary electrophoresis. The theory of capillary electrophoresis will be discussed later. Several years ago, micromachining technology was used to prepare chemical analysis systems on glass chips utilizing electroosmotic pumping to drive fluid flow and electrophoretic separation (2). The micromachining of capillary channels on a planar substrates provides a way to fabricate miniaturized chemical analysis systems on a chip. Rapid separation of complex sample mixtures combined with sample handling steps (4), such as dilution and injection, provide a basis for more complex, miniaturized analysis systems. The application of micromachining techniques to the miniaturization of chemical analysis is very promising and may lead to the development of analytical laboratories on a chip.

The basic process of chip-based capillary electrophoresis is illustrated in Figure 1.1. The etched substrate, which will be described later, is covered with another piece of glass, and then bonded at high temperature. The channel is usually 10-30  $\mu\text{m}$  deep and 30-70  $\mu\text{m}$  wide and several centimeters long. The sample injection method is shown in Figure 1.2. ( a ) The separation channel is first filled with buffer solution. The sample solution is injected at a certain voltage, so the small part of the channel between the two T's is filled with sample solution. ( b ) Then high voltage is added on both sides of the separation channel. ( c ) The sample is

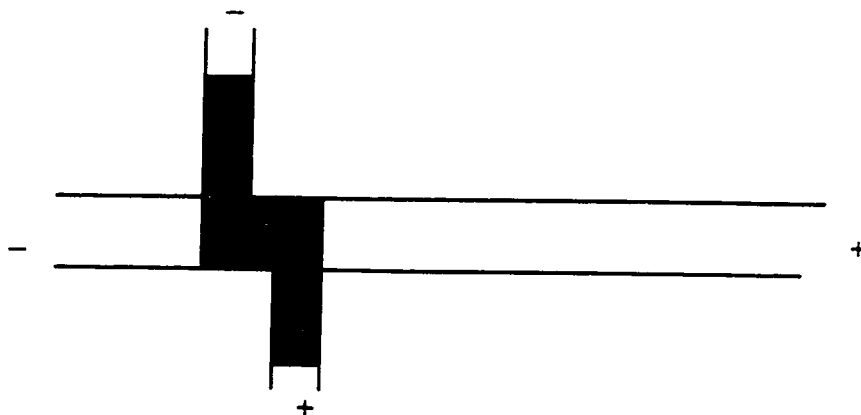


( a )

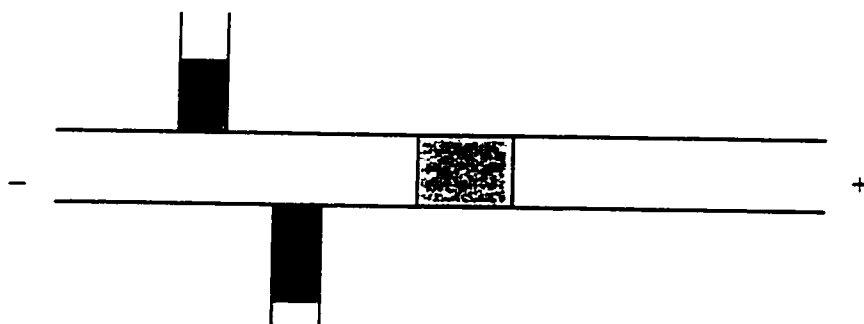


( b )

Figure 1.1 The basic structure of chip-based capillary



( a ) Sample solution fills the injection channel



( b ) Sample is injected



( c ) Sample is separated in the channel

Figure 1.2 The double T injection system



separated. These designs can be fabricated on a 3 inch or 4 inch square glass plate.

## 1.2 Detection Method

Absorbance and laser-induced fluorescence are the most generally used optical detection methods in capillary electrophoresis and liquid chromatography (5,6,7). Chemiluminescence has been studied (8,9,10,11), and some good results have been achieved. Laser-induced fluorescence has a low detection limit, but most samples do not have fluorescence signal, and must be labeled before detection. Some labeling processes are complicated, however, and some samples cannot be labeled. Consequently, absorbance is still a useful method for detection and is widely employed. The main problem with absorbance is its high detection limit. The absorbance detection limit is about  $10^{-6}$  M with commercial capillary electrophoresis instruments (12), while laser-induced fluorescence can give a limit of  $10^{-11}$  M (13). Improving the detection limit is a major challenge in absorbance detection.

Microchip-based capillary electrophoresis (CE) devices generally have such shallow channel depths that the sensitivity of absorbance with these devices is unsatisfactory. The Z-cell or U-cell device, as shown in Figure 1.3 which has been used in capillary electrophoresis and achieved good results, has been tested as a microfabricated device (7,14,15,16). A  $5 \times 10^{-5}$  M detection limit was achieved. Two problems were found with this microchip absorbance cell. First, a short separation distance ( $\sim 5$  cm), lead to thin detection plugs and thus, low signal. This is because a large detection volume will result in band broadening. The second problem is that the insertion of optical fibers within the chip is very difficult to achieve.

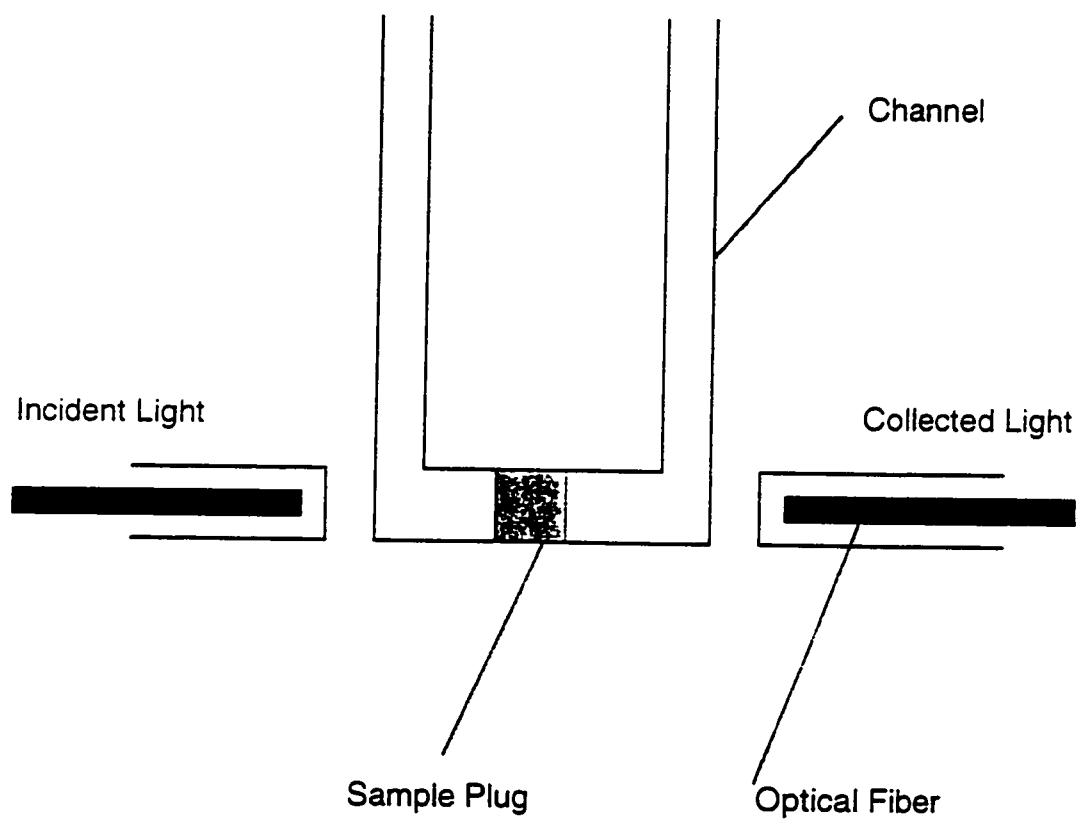


Figure 1.3 U-cell detection system

### **1.3 Micromachining**

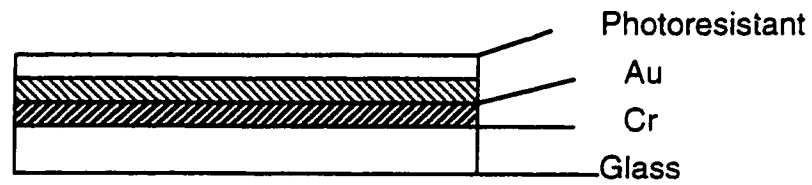
Micromachining refers to the fabrication of three dimensional micromechanical structures and related devices in silicon or other materials using microelectronic fabrication technology (17). Micromachining involves the processes of metal film deposition, photolithography, etching and bonding, all of which have been used in circuit manufacture(18,19). Using micromachining technology, many micromechanical structures have been fabricated and reported (17).

A standard one-mask fabrication process is outlined in Figure 1.4. A Cr, Au films are deposited on the substrate by vapor deposition or sputtering. Cr is deposited on glass to form an adherent layer. Au is used as a mask. A layer of photoresist, is usually spin coated on the surface. Residue solvent in the photoresist is removed by soft-baking at 120°C. Photolithographic patterning is then performed. The desired pattern is made on the master mask, with ultraviolet (UV) light usually being used as the radiation source. The exposed area of the photoresist undergoes photochemical reactions which change the physical and chemical property of the film so that can be patterned. There are two types of photoresist: positive and negative (20). For channel etching, a positive photoresist is used. After exposure, the exposed area is stripped off with developer solution. Then the metal mask and the substrate can be patterned by etching.

The strength of this technology in chemical analysis is that it can manufacture 3-dimensional structures. With this technology it is possible to fabricate reaction cells, separation cells and detection cells integrated onto a small substrate (4). Even heating elements can be incorporated.

### **1.4 Capillary Electrophoresis**

Electrophoresis has been widely used for many years for separating ionized compounds (21,22). Capillary electrophoresis(CE) was first used about 20 years ago



( a ) The glass is coated with Cr, Au and photoresistant



( b ) The photoresistant is exposed to UV light thereby removing the desired region



( c ) The exposed Au is removed using commercial aqua regia



( d ) The exposed Cr is removed using commercial Cr etch



( e ) The exposed glass is etched using  $\text{HF}/\text{HNO}_3/\text{H}_2\text{O}$



( f ) The remaining photoresistant Au and Cr are stripped

Figure 1.4 One mask fabrication process

by Viranen and Mikkers *et al.* and popularized by Jorgenson and Luckacs(23,24,25,26,27). Capillary electrophoresis is currently emphasized in scientific research because of its low sample consumption, high resolution, and efficient separation. A variety of CE instruments have been commercially available in recent years (28).

Several types of capillary electrophoresis have been studied. The most common type of capillary electrophoresis is capillary zone electrophoresis (CZE). Others are capillary gel electrophoresis (CGE), capillary isoelectric focusing (CIEF), and micellar electrokinetic chromatography (MEKC). The basic concept of capillary electrophoresis is illustrated in Figure 1.5 (28,29)..

Capillary zone electrophoresis is the most common type of capillary electrophoresis. The capillary is usually made of fused silica with 10-100  $\mu\text{m}$  inner diameter and 30-100 cm lengths and is filled with a fixed pH buffer solution. High voltage is applied on the two sides of the capillary to pump the solution from one side to the other. Samples are injected from the inlet side. Because of the different electrophoretic mobility of the samples in the capillary, they are separated during migration in the electric field.

The capillary is often washed with 0.1 M NaOH. This NaOH changes the  $-\text{Si}-\text{O}-\text{H}$  on the capillary surface to  $-\text{Si}-\text{O}^-$ , making the surface of the capillary negatively charged (30). This reaction creates an electrical double layer on the surface of the capillary. The potential difference near the wall is called the zeta potential,  $\zeta$ . When a voltage is applied across the capillary (31), the solution moves to the cathode, drawing the bulk solvent along with it. This solvent movement is termed the bulk flow or electroosmotic flow (EOF). Because of the existence of the electrical field in the capillary, all charged particles are affected by it. Positively charged particles move to the cathode, and negatively charged particles move to the anode. Neutral particles move with the bulk flow. Figure 1.6 shows the movement of the particles (32). Because the sample particles are charged differently, their direction of motion may be different. The separation of ions is determined by the

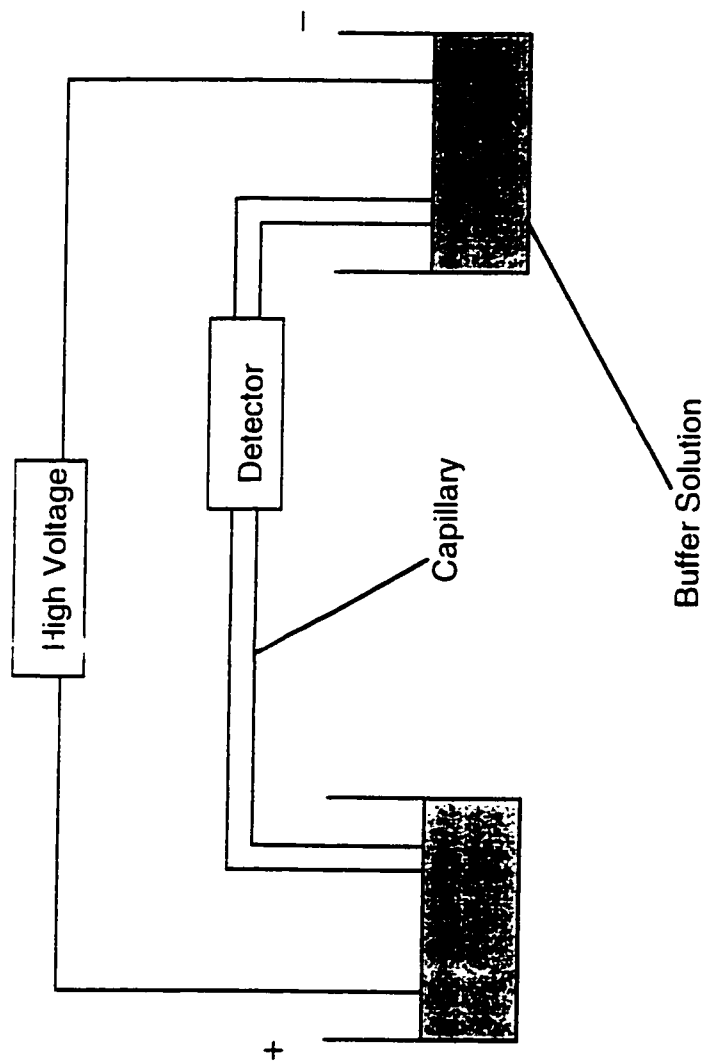
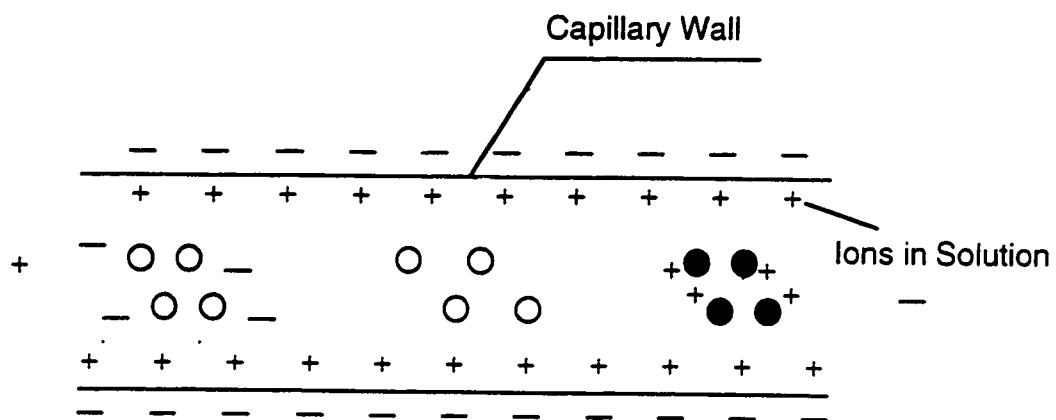
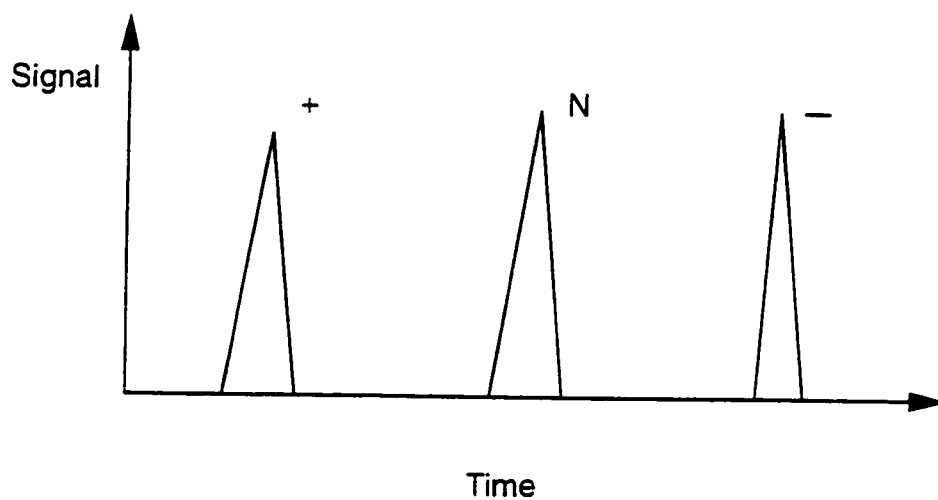


Figure 1.5 General schematic of a conventional CTE instrument



( a ) The separation of differently charged particles



( b ) Detected peak sequence of differently charged particles

Figure 1.6 Diagram illustrating the separation of charged and uncharged species in capillary electrophoresis

net velocity or mobility difference, which can be describe as:

$$\mu_n = \mu_{eo} + \mu_{ep} \quad (1.1)$$

$$\mu_{eo} = \epsilon \zeta / 6 \pi \eta \quad (1.2)$$

$$\mu_{ep} = q / 6 \pi \eta \gamma \quad (1.3)$$

where  $\mu_n$  is the net mobility of the particle,  $\mu_{eo}$  is the bulk flow mobility or electroosmotic flow mobility, and  $\mu_{ep}$  is the sample particle mobility or electrophoretic mobility in the presence of an electric field.  $\zeta$  is the zeta potential.  $\epsilon$  is the dielectric constant,  $\eta$  is the viscosity of the solution,  $q$  is the charge and  $\gamma$  is hydrodynamic radius of the ion (33,34). Because the bulk flow mobility is usually higher than the electrophoretic mobility, all sample particles normally move to the negative electrode. The flow sequence is thus positively charged particles, neutral particles and negatively charged particles. This is why differently charged particles can be separated and detected at the same detector location. Because the surface charge and hence the zeta potential is affected by the buffer pH, the mobility of the solution changes with pH (35,33). Normally, capillary zone electrophoresis is performed in pH>3 buffer solution.

The  $\zeta$  potential is a function of pH, increasing as pH increases and a function of the ionic strength of the buffer, decreasing as the ionic strength increases(36,29). With increasing pH, the magnitude of negative charge on the wall of capillary will increase. Increasing ionic strength will decrease this electrical double layer effect. At low pH, pH<3, the capillary wall will be positively charged. The electroosmotic component of velocity will then be reversed, since the double layer will have a net negative charge and will migrate towards the anode.

Another important issue in chromatography separation analysis is the influence



of band broadening. In capillary electrophoresis, the main effect of bandbroadening results from longitudinal diffusion (25,26). Equation (1.4) gives the relationship of migration time with net mobility of the particles, applied voltage, and the capillary length between injector and detector.

$$t=L^2/\mu_n V \quad (1.4)$$

where  $t$  is migration time,  $L$  is the capillary length between injector and detector,  $\mu_n$  is the net mobility of the sample particles, and  $V$  is the applied voltage. The plate number equation shows the relationship more clearly,

$$N=\mu_n V/2D \quad (1.5)$$

where  $N$  is the plate number, and  $D$  is the diffusion coefficient. This equation is obtained only when longitudinal diffusion is the major source of band broadening and other sources are negligible.

From the above equation, it can be seen that a high voltage will give a high plate number or increase the separation efficiency. In capillary electrophoresis, Joule heating will be a problem at high voltage. Because of the resistance of the solution, the solution will be heated at high voltage, resulting in density and temperature gradients which will increase the band broadening and even break down the electrophoresis process if the solvent boils.

## 1.5 Multi-Reflection Absorption Cells

Multi-reflection spectroscopy is a type of internal reflection spectroscopy. It is a technique in which a beam is reflected many times through a sample in order to increase the path length for absorbance, and so improve the sensitivity. A high reflectance material is often coated on both sides of a sample cell. The incident light

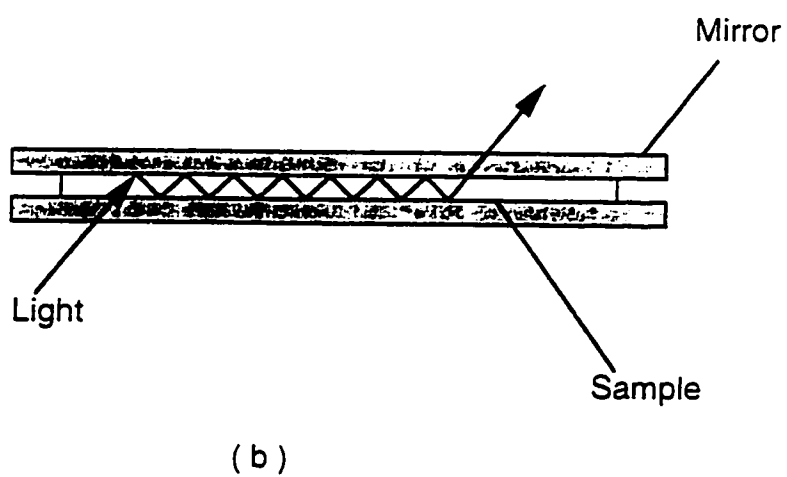
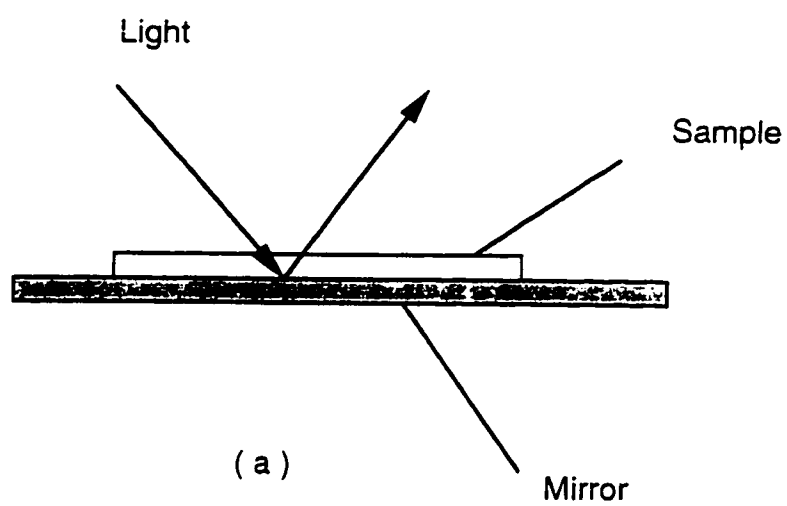


Figure 1.7 Diagram of internal reflection absorbance cell

accesses from one side, and then reflects multiple times between the mirrors, as shown in Figure 1.7 b. This technique is useful for increasing the sensitivity of measurement of thin films, like monolayers, or of low concentration solutions or gases .

The use of multi-reflection designs to increase absorbance sensitivity can be traced back to 1942 (37,38,39,40). Authors have reported a multi-reflection cell formed on a fused silica capillary in CE (41), while the longitudinal transmission in Z-cell- and U-cell-shaped capillaries has also demonstrated increased optical path lengths in CE. A silicon-based absorbance detection cell has been described by Verpoorte *et al.* in which multi-reflection could be performed (42).

Multi-reflection spectroscopy is an effective method in infrared spectroscopy. In infrared spectroscopy, the sample is coated on a plate of Ge, Si or KRS-5. Figure 1.8 shows the structure of the plate and the light direction. Because of the high index of refraction of the plate material, the light is totally reflected on the surface of the plate when the light is incident at the critical angle for that material. This method is called attenuated total reflection infrared spectroscopy (ATR-IR). Samples are coated on the two surfaces of the substrate. Monolayer Langmuir-Blodgett film has been detected and studied with this method. This is an effective method in thin film study and surface study because of its high sensitivity.

## 1.6 Scope of Present Work

In this thesis we develop methods to fabricate a multi-reflection absorbance cell that can be micromachined for our microchip-based CE system. The results prove that the multi-reflection absorbance cell has higher sensitivity and is more convenient to make than the micro-fabricated U-cell systems.

The theory and design will be described in Chapter 2. The basic theory of multireflection is described by Lambert's and Beer's Law. The purpose of a multireflection cell is to increase the path length of the incident beam in the sample.

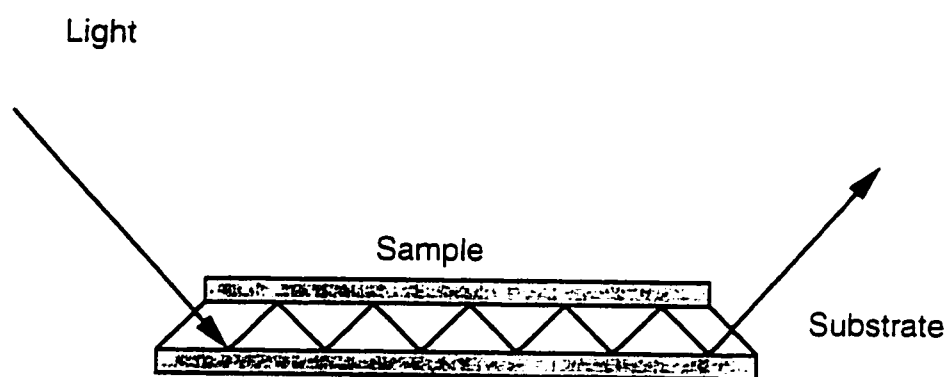


Figure 1.8 Attenuated Total Reflection infrared absorbance cell

In our experiments two different designs were tested. The reasons for and details of these designs will be discussed in this chapter.

Chapter 3 describes some bonding tests. Because for our designs, low glass bonding temperature, short bonding time and multiple-piece bonding were needed. These tests include a cleaning step, proper bonding conditions and bonding quality.

Chapter 4 is focused on choices of the metal for mirrors. In this multireflection absorbance cell a metal film is used as both reflection mirror and light mask. The other parameter is the thickness of the metal film, which cannot be too large, because the metal film will be sandwiched between two glass plates. Several metals and several parameters, including reflectivity and transmission with metal film of different thicknesses, were tested.

Chapter 5 reports the entire cell fabrication and characterization of the cleaning of the Al coated glass and hole drilling on bonded glass.

Chapter 6 describes some experiments used to characterize the new absorbance cell. The detection system, test procedure and result will be discussed in this chapter.

## References

1. Harrison, D. J.; Manz, A.; Fan, Z.; Ludi, H.; Widmer, H. M. *Anal. Chem.* 1993, 64, 1926.
2. Harrison, D. J.; Seiler, K.; Fan, Z.; Effenhauser, C.S.; Manz, A. *Science* 1993, 261, 895-897.
3. Harrison, D. J.; Fan, Z. H. *Anal. Chem.* 1994, 66, 177-184.
4. Harrison, D. J.; Seiler, K.; Fan, Z. H.; Fluri, K. *Anal. Chem.* 1994, 66, 3485-3491.
5. Zare, R. N.; Gassmann, E. *Eur. Pat. Appl. EP* 21660, 1987.
6. Cheng, Y-F.; Dovichi, N. *J. Science* 1988, 242, 562-564.
7. Chervet, J. P.; Van Soest, R. E. J.; Ursem, M. *J. Chromatogr.* 1991, 543, 439-449.
8. Nieman, T. A. *Encyclopedia of Analytical Science*; Townshend, A., Ed.; Academic Press, 1995; Vol. 1, pp 608-621.
9. Rongen, H. A. H.; Hoetelmans, R. M. W.; Bult, A.; Van Bennekom, W. P. *J. Pharm. Biomed. Anal.* 1994, 12, 433-462.
10. Sanchez, F. G.; Diaz, A. N.; Garcia, J. A. G. *Journal Of Luminescence* 1995, 65, 33- 39.
11. Mangru, S. D. M. S. Thesis, Dept of Chem. University of Alberta. 1997.
12. Chen, F. T. A.; Pentoney, S. L. *J. Chromatogr. A* 1994, 680, 425-430.
13. Ocirk, G.; Tang, T.; Harrison, D.J. *Analyst*, July 1998, Vol. 123 ( 1429-1434 ).
14. Bruin, G. J. M.; Stegeman, G.; Van Austen, A. C.; Xu, X.; Kraak, J. C.; Poppe, H. *J. Chromatogr.* 1991, 559, 163-181.
15. Moring, S. E.; Reel, R. T.; Van Soest, R. E. *J. Anal. Chem.* 1993, 65, 3454-3459.
16. Liang, Z.; Chiem, N.; Ocirk, G.; Tang, T.; Fluri, K.; Harrison, D. J. *Anal. Chem.* 1996, 68, 1040-1046.
17. Delapierre, G. *Sensors and Actuators*, 1989, 17, 123-138.

18. Gise, P. E.; Blanchard, R. B., *Semiconductor and Integrated Circuit Fabrication Techniques*, Peston Publishing Co.: Reston, VA, 1979.
19. Ko, W. H.; Suminto, J. T., in *Sensor: A Comprehensive Survey*, Grandke, T.; Ko, W. H., Eds; *VCH Press*: Weinheim, Germany, 1989, 1, 107-168.
20. Weill, A., in *The Physics and Fabrication of Microstructures and Microdevices*, Kelly, M. J.; Weisbuch, C., Eds; *Springer-Verlag: Berlin*, 1986, 59-64.
21. Tiselius, A., *Trans. Faraday Soc.*, 1937, 33, 524-531.
22. Hjerten, S., *Chromatogr. Rev.*, 1967, 9, 122-224.
23. Virtanen, R., *Acta Polytech. Scand. Chem. Include. Metall. Ser.*, 1974, 123, 1-67.
24. Mikkers, F. E. P.; Everaerts, F. M.; Verheggen, Th. P. E. M., *J. Chromatogr.*, 1979, 169, 11-20.
25. Jorgenson, J.; Lukacs, K. D., *Anal. Chem.* 1981, 53, 1298-1302.
26. Jorgenson, J.; Lukacs, K. D., *Science*, 1983, 222, 266-272.
27. Gordon, M. J.; Huang, X.; Pentoney, S. L.; Zare, R. N., *Science*, 1988, 242, 224-228.
28. Terabe, S., *Anal. Chem.* 1990, 62, 605A-607A.
29. Cooky, K. *The Separation Times*, 1993; Vol.7.
30. Lukacs, K. D.; Jorgenson, J., *J. HRC & CC* 1985, 8, 407-411.
31. Deyl, Z.; Everaerts, F. M.; Prusik, Z.; Svendsen, P. J. *Journal of Chromatography Library* Vol. 18 5-8.
32. Cooksy, K. In *The Separation Times*. 1993, Vol. 7.
33. Ewing, A.; Wallingford, R. A.; Olefirowicz, T. M., *Anal. Chem.* 1989, 61.
34. Chien, R.; Burgi, D. S., *Anal. Chem.* 1992, 64, 489A-496A.
35. Lee, C. S. *Handbook of Capillary Electrophoresis*; Landers, J. P., Ed.; *CRC Press*, 1997.
36. Lee, C.S. In *Handbook of Capillary Electrophoresis*; Landers, J. P., Ed.; *CRC Press*, 1997.
37. White, J. U. *J. Opt. Soc. Am.* 1942, 32, 285-288.

38. Bernstein, J. H.; Herzberg, G. *J. Chem. Phys.* 1948, 16, 30-39.
39. Pilston, R. G.; White, J. U. *J. Opt. Soc. Amer.* 1954, 44, 572-573.
40. Gould, J. H. *Appl. Spectrosc.* 1971, 25, 103-105.
41. Wang, T.; Aiken, J. H.; Huie, C. W.; Hartwick, R. A. *Anal. Chem.* 1991, 63, 1372-1376.
42. Verpoorte, E.; Manz, A.; Ludi, H.; Bruno, A. E.; Maystre, F.; Krattiger, B.; Widmer, H. M.; van der Schoot, B. H.; de Rooij, N. F. *Sensors and Actuators B* 1992, 6, 66-70.



## **Chapter Two : Theory and Design**

### **2.1 Introduction**

Absorption spectroscopy is an important method of analysis. The basic concept behind absorption spectroscopy is Beer and Lambert law, which gives the relationship between absorption, concentration and path length. To decrease the detection limit, the most convenient method is to increase the pathlength. The multiple reflection absorption cell is one of the most effective methods and has been commercially used in infrared (IR) and other analysis systems (1,2).

In this work, we designed a new absorption cell based on the idea of multiple reflection for application to microchip-based capillary electrophoresis. This chapter discuss the basic theory. More details on design and the measurement system will be discussed later.

### **2.2 Beer and Lambert Law**

From the work of Lambert and Beer, we know the relationship between absorption and path length and between absorption and concentration. These relationships may be expressed as:

$$E = \log I/I_0 = abc \quad (2.1)$$

Where E is extinction or the logarithm of the ratio of the incident to the transmitted intensity of light. Lambert's law more specifically indicates that the extinction, E, is a linear function of b, the path length of the light in the material. Beer's law

indicates that the extinction is a linear function of the concentration,  $c$ , of the material.  $a$  is a constant of proportionality for the specific sample.

## 2.3 Multi-reflection Cell Considerations

The multiple reflection method has been used in several other related fields to increase the path length. Figure 2.1 illustrates the configuration of our microchip-based multi-reflection absorbance cell. In this cell design, the metal was deposited on the glass substrate to form a reflective mirror. The incident light is reflected on the mirror and then passed through the channel which is located at the center of the two pieces of glass.

The incident beam is refracted at each medium interface of glass-air and glass-solution and is reflected at the mirrors. For each reflection of the light, the beam passes through the channel a distance  $L_3$  and the glass a distance  $L_2$ ,  $L_4$ . Equation 2.2 shows the relationship of  $L_1$  with the thickness or channel depth and incident angle  $\theta$ :

$$L_1 = h_i / \cos\theta \quad (2.2)$$

where  $L_1$  is the path length of the light in the channel or in the glass,  $h_i$  is the thickness of the region,  $\theta_i$  is angle of the light within the medium with respect to the surface normal, and  $i$  refers to the medium as identified in Figure 2.2

For each path length, the longitudinal travel,  $l_i$ , is given by:

$$l_i = h_i \tan\theta_i \quad (2.3)$$

The total longitudinal travel for each reflection,  $l$ , is given by:

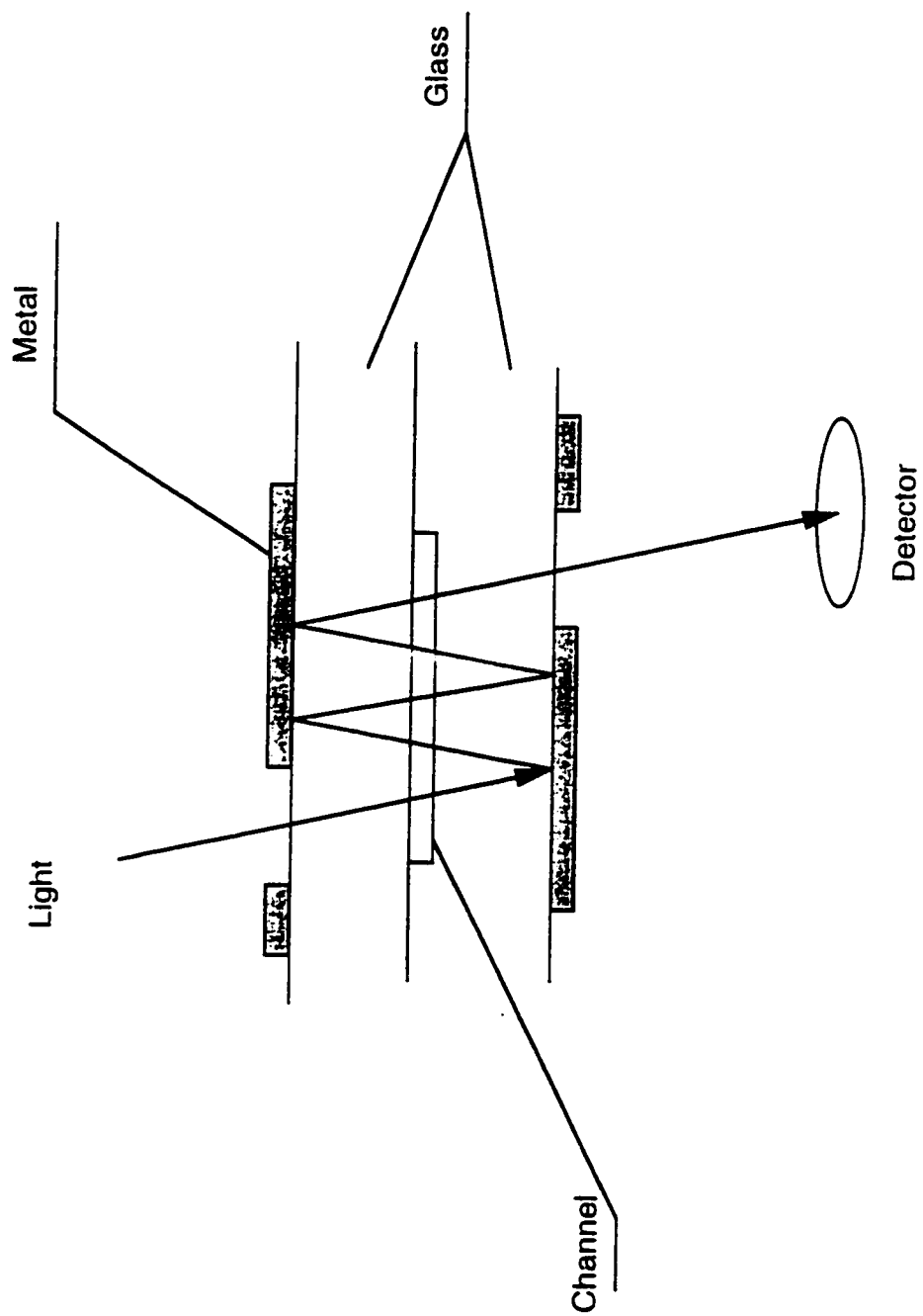


Figure 2.1 Multiple reflection absorbance cell on microchip-based capillary

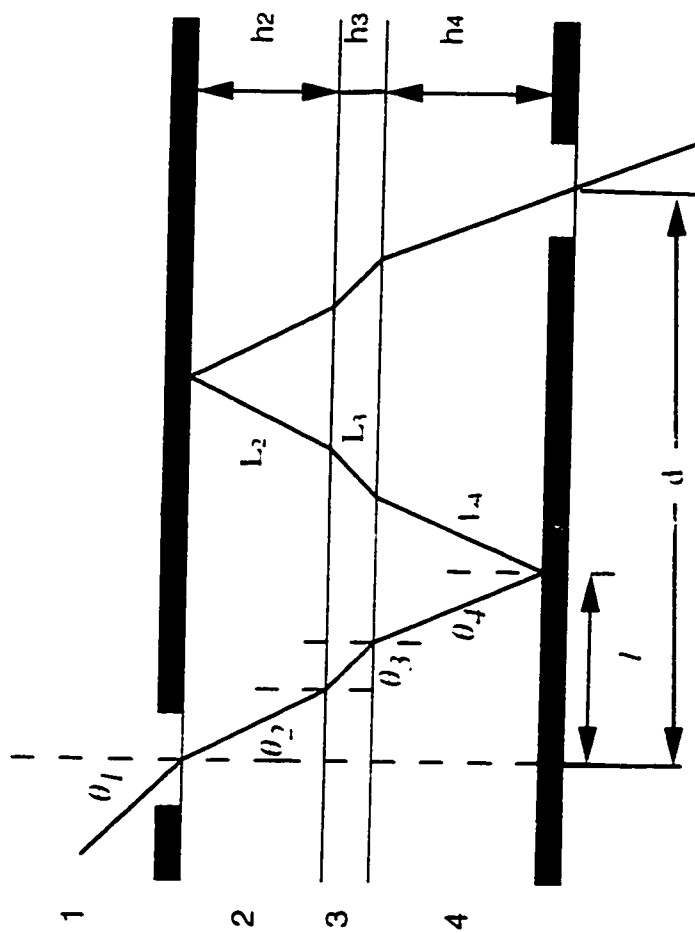


Figure 2.2 Relevant dimensions and angles for determining optical path length

$$l = l_2 + l_3 + l_4 \quad (2.4)$$

and the total reflection number,  $N$ , is given by:

$$N = d/l \quad (2.5)$$

where  $d$  is the distance between the entrance and exit apertures. The total theoretical path length for absorbance within the multi-reflection cell,  $L$ , is given by:

$$L = Nl_3 = Nh_3/\cos\theta_3 \quad (2.6)$$

where  $h_3$  is the depth of the channel.

The path length of the light in the sample is affected by reflection number and depth of the channel. The reflection number is affected by the incident angle, the thickness of the glass and the distance between entrance and exit apertures. The distance between the apertures is limited by the injection plug and separation distance. A 200  $\mu\text{m}$  length was chosen in our experiment. Theoretically, a lower incident angle will increase the path length. But only certain angles can give maximum light throughput. This will be shown in Chapter 6.

Figure 2.3 shows the plots of path length versus the incident angle and the reflection number versus the incident angle. We used 75  $\mu\text{m}$  and 200  $\mu\text{m}$  thick glass because these were the thinnest substrates commercially available. It is clear that increasing the depth of the channels can have as much influence as reducing the thickness of the glass. Since preparing and handling thin glass pieces can make device fabrication difficult, it may be advantageous to use deeper channels and thicker glass.

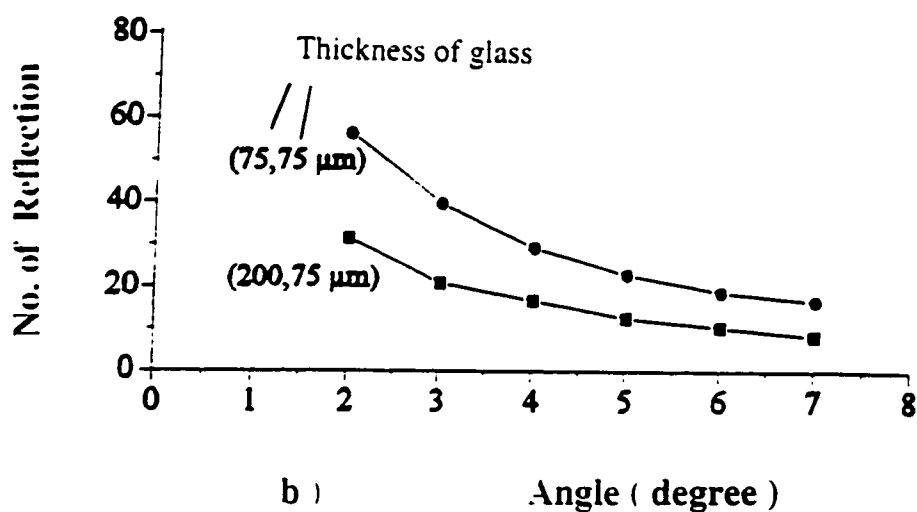
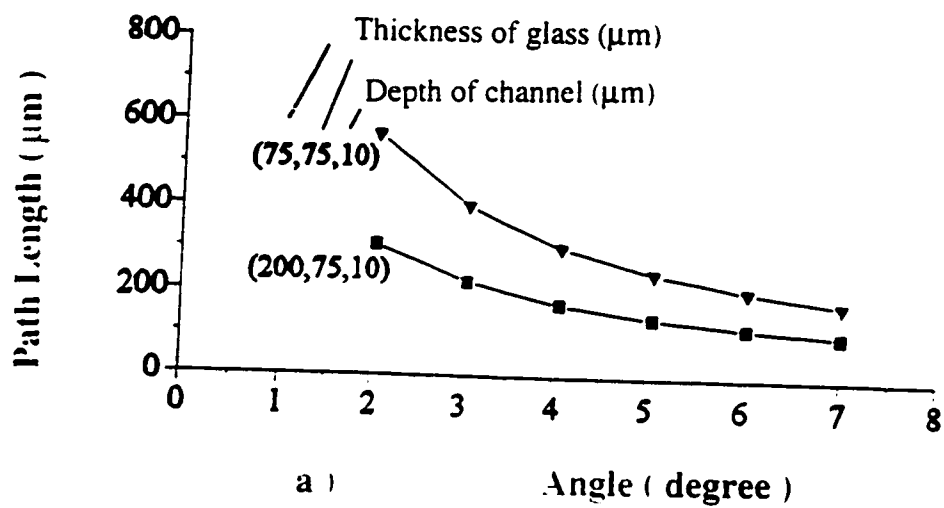


Figure 2.3 Calculation for multireflection cell

- a ) Plot of the calculated path length as function of the incident beam angle
- b ) Plot of the calculated number of reflection versus incident beam angle

## **2.4 Absorbance Cell Design**

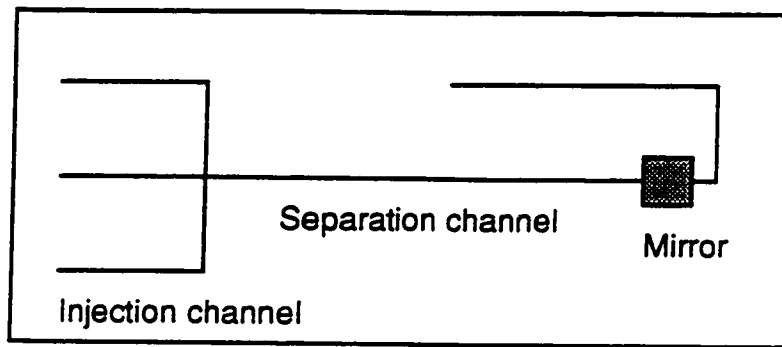
### **2.4.1 Mirror and Aperture Design:**

The basic purpose of a multi-reflection absorbance cell is to increase the path length of the light through the sample. In a microchip-based device, the separation distance of the channel is 3 to 5 cm (3). The longitudinal distance of the incident light path cannot be too long compared to this distance or else the detection volume will lead to band broadening. A distance of 200  $\mu\text{m}$  between incident aperture and detection aperture was selected for this study since this length should be short enough that the detector volume does not contribute significantly to band broadening.

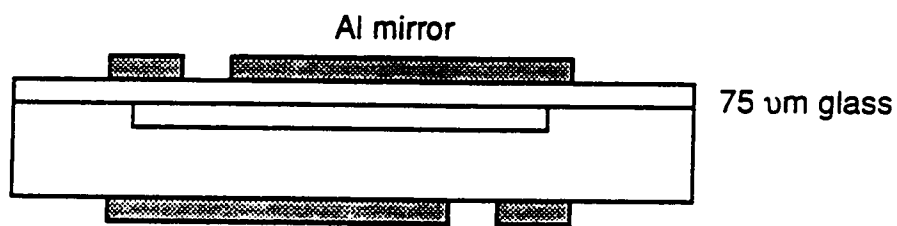
To prevent incident light from reaching the detector, a small hole on a large square metal mirror was used to block out the stray light that came from the incident beam, mirror reflection and glass scattering. The 1  $\text{cm}^2$  square mirror is bigger than the window of the detector so it can mask the detector from stray light. The hole has the same width as the channel and is located above top of the channel.

### **2.4.2 Design 1**

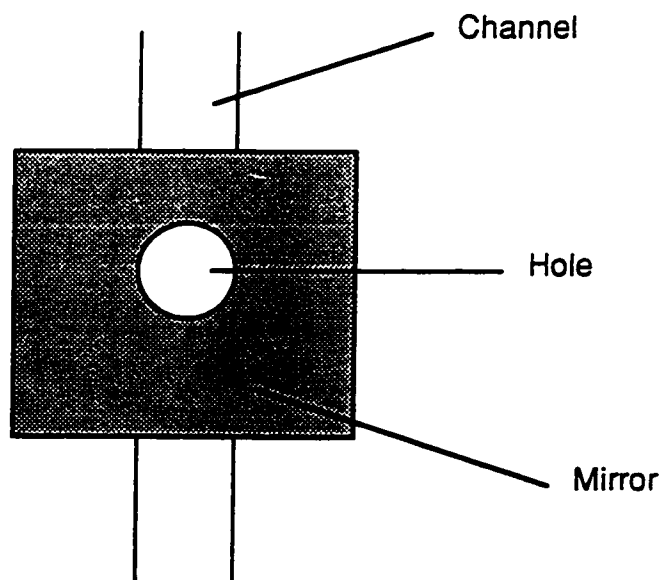
Figure 2.4 ( a ) shows the top view of the chip. Figure 2.4 ( b ) illustrates the side view of the chip. In this design, the 200  $\mu\text{m}$  0211 glass was chosen as the substrate, since it can survive the lithographic process. Channels were etched on it and access holes were drilled into it. A piece of 75  $\mu\text{m}$  glass was used as cover glass. After bonding the cover slip, a metal mirror was deposited on both sides of the chip and the light apertures were patterned. Figure 2.4 ( c ) shows the enlarged metal part of design 1. For the metal pattern, the same mask was used on both sides.



( a )



( b )



( c )

Figure 2.4 Design 1 ( a ) Top view of the chip ( b ) Side view of the chip  
( c ) Top view of the mirror



### **2.4.3 Design 2**

In design 1, the total thickness of the chip after bonding was 275  $\mu\text{m}$ . Compared with the 10  $\mu\text{m}$ -deep channel, the chip was still too thick, since most of the longitudinal travel of the beam would still be in the glass. The thickness of the substrate needed to be reduced to increase the contribution of each reflection to the optical path length.

In design 2, the same mask was used, but a sandwich structure of 200, 75 and 200  $\mu\text{m}$  or 500  $\mu\text{m}$  thick glass was formed with one of the mirror inside the sandwich. The 200  $\mu\text{m}$  wafer was used as a handle wafer to provide physical support for the 75  $\mu\text{m}$  thick glass. First a metal mirror was formed on the 200  $\mu\text{m}$  thick wafer, then the 75  $\mu\text{m}$  thick glass was bonded on top of this mirror. The top of the 75  $\mu\text{m}$  glass was then lithographically patterned to form the flow channel, and access holes were drilled through this 275  $\mu\text{m}$  thick assembly. Cover glass 75  $\mu\text{m}$  thick was bonded on top of the channel. The top layer of the metal mirror was then deposited and patterned on the cover glass. Figure 2.5 illustrates the design. By design 2, the total thickness of chip change to 150  $\mu\text{m}$  while the thickness is 275  $\mu\text{m}$  in design 1. Both the pass length and reflection number increase are shown in Figure 2.3.

## **2.5 Fabrication Issues**

Because Al will be oxidized during the high temperature bonding stage, it is deposited and patterned after bonding in design 1. In design 2 the first layer of Al

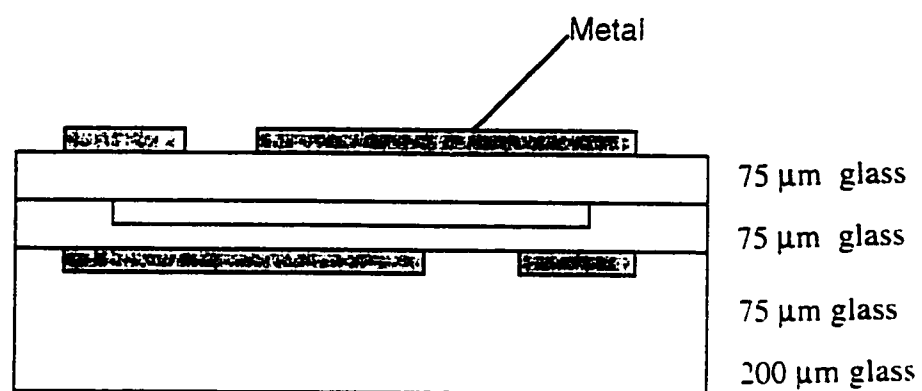


Figure 2.5 Design 2

has to be sandwiched between the glass before bonding and we have to bond three pieces. This procedure causes the following questions: 1. Will the first layer of Al will be oxidized or not? 2. How does the Al film affect the bonding ? 3. Will bonding the third piece be affected by bonding the first two pieces, and vice versa? All the details of these problems will be discussed in later chapters.

## References

1. Verpoorte, E.; Manz, A.; Ludi, H.; Bruno, A. E.; Maystre, F.; Krattiger, B.; Widmer, H. M.; van der Schoot, B. H.; de Rooij, N. F. *Sensors and Actuators B* 1992, 6, 66-70.
2. Wang, T.; Aiken, J. H.; Huie, C. W.; Hartwick, P. A. *Anal. Chem.* 1991, 63, 1372-1376.
3. Fan, Z. H.; Harrison, D. J. *J. Anal. Chem.* 1994, 66, 177-184.

## **Chapter Three: Glass Bonding Procedures**

### **3.1 Introduction**

Glass devices are fusion bonded at high temperature, which can give better bonding quality. However, too high a temperature will damage the glass, while too low a temperature may not lead to bonding. Consequently, the best bonding conditions had to be determined.

In our test, Al was chosen as the mirror material for reasons that will be discussed in Chapter 4. At a high temperature, Al was oxidized and black spots formed, damaging the mirror. The Al therefore must be deposited after chip bonding. This raises a new problem: the glass substrate shrinks in the bonding stage. This shrinkage makes the alignment of the metal pattern difficult. Because the shrinkage is proportional to the bonding temperature and bonding time, the lowest temperature and shortest bonding time must be used.

### **3.2 Previous Bonding Conditions for 0211 Glass**

Because 0211 glass has similar properties to those of mask glass, we usually used a mask glass temperature program developed in our group to bond 0211 glass. The program is given below in Table 3.1. Our search for a new bonding program started with the program in Table 3.1.

**Table 3.1 Previous Bonding Condition of Mask Glass**

	Rate ( °C/min )	Temp ( °C )	Time ( Hrs. )
Stage 1:	10	440	0.5
Stage 2:	2	475	0.5
Stage 3:	2	592	6.0
Stage 4:	4	473	0.5

### **3.3 Experiment**

#### **3.3.1 Material**

Corning 0211 glass with a thickness of 75  $\mu\text{m}$  is the thinnest available. In our final chip, we used 200  $\mu\text{m}$  glass as substrates. Both 75  $\mu\text{m}$  and 200  $\mu\text{m}$  thick glass were chosen as test substrates.

#### **3.3.2 Cleaning**

The glass substrate was washed in pirhana solution (concentrated  $\text{H}_2\text{SO}_4$ :  $\text{H}_2\text{O}_2$ =3:1) (1) for half an hour and then cleaned with distilled water. This cleaned glass was washed with a Model 2066 Microautomation (Fremont CA) pressure rinser in a class-100 cleaning station until no particles prevented contact between the glass plates. These contacted glass plates were then put in an oven for the bonding test.

### **3.3.3 Bonding Conditions and Bonding Testing**

In a mask glass bonding program, the highest temperature is 592 °C (2), at which the glass is heated for 6 h. The new tests start at 590 °C for 6 h. To shorten the bonding time, we used one stage instead of the four list in Table 3.1. To decrease the preheating time, we chose a heating rate of 10 °C/min.

A qualitative testing of the bonding was performed by using a Si wafer scribing pen with a tungston carbide tip. The wafer was held firmly on a flat surface and the scribing pen tip was forced into the bond to try to pry the plates apart. With good bonds this effect was unsuccesful. With poor bonds the plates came apart, or interference fringe could be made to appear near the tip, indicating partial separation of the plates.

#### **a. Bonding Time Test**

As described previously, the test started at 590 °C for 6 h in 1 stage. The heating rate was 10 °C/min. The bonding time was then decreased by 0.5 h intervals until the condition used was 590 °C for 0.5 h. The pieces of glass were still bonded. Finally, we found the glass could still be bonded at 590 °C, with only 0.3h at this temperature, and a 10 °C/min ramp up to 590 °C.

#### **b. Bonding Temperature Test**

After the bonding time test, the lowest bonding temperature was tested. The test started at 590 °C for 0.3 h, and then the temperature was lowered by 10 degree steps. The lowest temperature at which the glass could be bonded was 450 °C. At 440 °C, 1 h, 2 h and longer times were tested, but the glass was not bonded.

### c. Other Test

In normal glass bonding programs, we usually have a stage to control the glass cooling speed, as we did in stage four of the mask glass bonding program. The pieces of glass were left in the oven for several hours until they were cooled down to nearly room temperature. If the glass is taken out of the oven at high temperature, it tends to break or crack.

In this new program, we tried to leave the glass in the oven for as short a time as possible, because with the old method the oven remained hot for a long time after the heating stopped. The long time at high temperature affected the glass by causing more shrinkage. With the cooler, shorter bonding procedure we could take the glass out of the oven just as the heating stopped. All test glass survived. In our experiment, no chips were broken with the new procedure.

### d. Conclusion

For Corning 0211 glass, the bonding condition can be set as Table 3.2:

Table 3.2 Bonding Condition of 0211 Glass

Rate (°C/min)	Temperature (°C)	Time (hr.)
10	450	0.5

with these conditions, the bonded glass can be taken out of the oven immediately after the heating stops.

### 3.4 Three-Piece Bonding Test

#### 3.4.1 Introduction

In design 2, the third piece of glass was bonded after the metal was sandwiched between the first two layers. In the first bonding step, glass was heated to 450 °C. However, the inner structure and chemical properties of the glass may change after bonding, thus affecting the bonding of the third piece at a later stage. If the property of the glass changes as a result of bonding conditions, some treatment may have to be done before bonding the third piece. To evaluate this possibility bonding tests for the third piece were done.

#### 3.4.2 Bonding Test

200 µm and 75 µm 0211 glass were chosen for testing, and both pieces of glass were cleaned with  $\text{H}_2\text{SO}_4:\text{H}_2\text{O}_2=3:1$  and high pressure water. The 200 µm thick glass and the 75 µm thick glass were bonded at 450 °C for 0.5 h. This bonded pair and another piece of 75 µm thick glass were cleaned in  $\text{H}_2\text{SO}_4:\text{H}_2\text{O}_2=3:1$  and with high pressure water. They were then contacted and bonded at 450 °C for 0.5 h. They bonded well, meaning that a temperature of 450 °C did not affect the bonding property of the glass significantly. As a result, we used the same bonding condition to bond the third piece. This bonding method was used in all subsequent experiment and no problem with separation ever occurred.

### References

1. Fan, Z. H.; Harrison, D. J. *Anal. Chem.* 1994, 66, 177-184.
2. Chiem, N. Ph.D Thesis, Dept. of Chem. U. of Alberta. 1997.



## **Chapter Four: The Choice of Metal for Mirrors**

### **4.1 Introduction**

In a multi-reflection cell, reflective losses can lead to very poor light throughput when the reflection number is high, so it is important to use a high quality mirror. Several metals compatible with the method for manufacturing thin-film integrated circuits were evaluated. Several parameters were important, including the reflectivity and the transmission, since the mirror was also used as a light mask for the detector. Achieving good performance with thinner films is also important, because for design 2 the glass had to be able to deform around the metal film mirror in order to bond.

To increase the intensity of the detector light, a high reflectance metal had to be used. Figure 4.1 (1) illustrates the reflectance of some metals. Ag, Au and Cu and Al have high reflectance at 633 nm, at which our test was done. But Ag, Au and Cu do not adhere well to glass. Because Au is stable, it is used widely in the microelectronic industry. Even in our normal glass etching process, it is used as a mask. However, to use Au, Cr is deposited on the glass first to form an adherent layer for the Au film (2). As a result the Cr forms the mirror and not the Au, and Cr makes a poorly reflective mirror.

A simple method was tried to decrease the effect of Cr reflectivity by using a thinner Cr film as an adherent layer. A 133 Å Cr film with a thicker Au layer was tested.

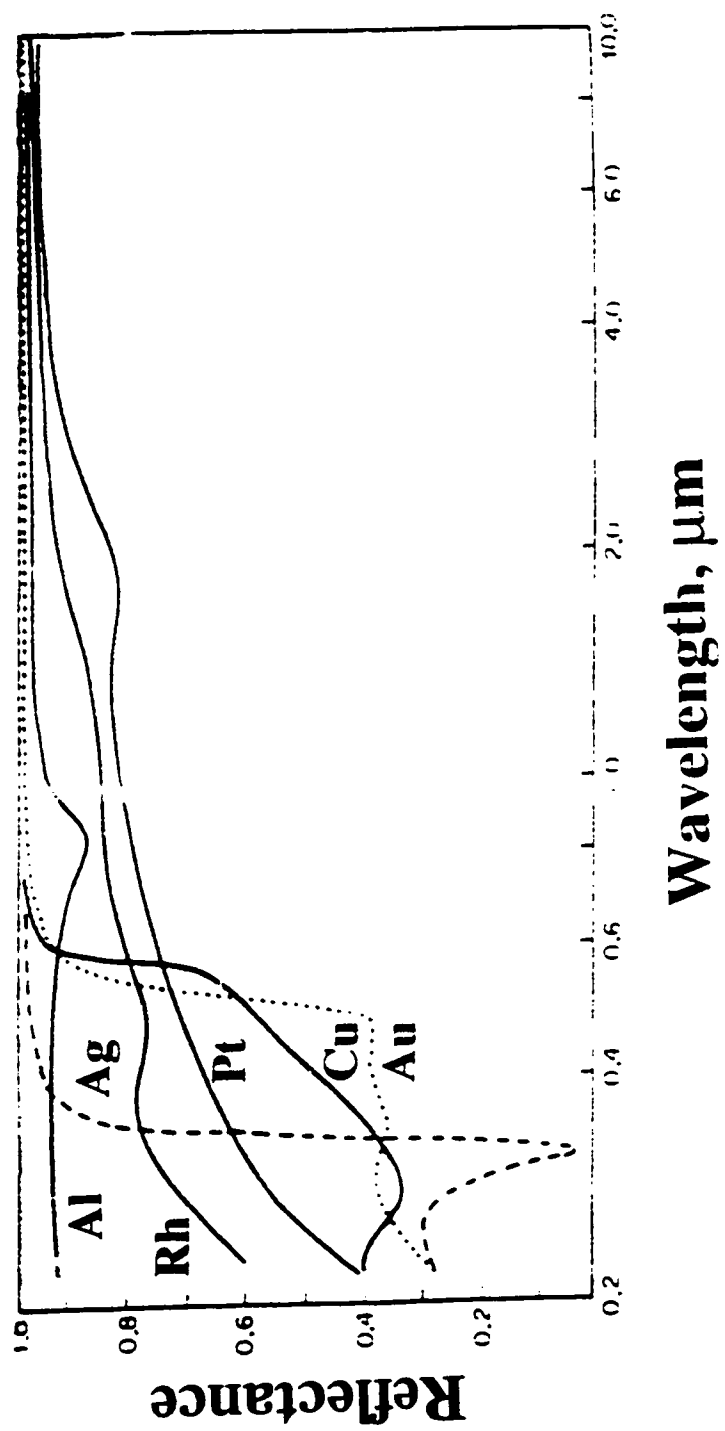


Figure 4.1 Spectral reflectance of certain metals(1)

## 4.2 The Method for Determining the Absolute Reflectance of Metallic Films

The reflectance of metallic films is one of their important physical properties. The absolute reflectance of a material can be determined from the measurement of the relative reflectance of the material when referenced to a standard reference material. When the absolute reflectance of the reference material is known, the absolute reflectance of the sample material can be calculated.

### 4.2.1 Theory

The theoretical absolute reflectance of materials illuminated by light incident at 90 degrees to the surface of the material is governed by the Fresnel equation. For a surface of an absorbing material in air, the absolute reflectance of the bulk material is given by equation 4.1 (3):

$$R(\lambda) = \frac{[n(\lambda) - 1]^2 + [K(\lambda)]^2}{[n(\lambda) + 1]^2 + [K(\lambda)]^2} \quad (4.1)$$

In equation 4.1,  $R(\lambda)$  is the theoretical value of the absolute reflectance of the material in air when illuminated by light of wavelength  $\lambda$ . The absolute reflectance,  $R(\lambda)$ , is a function of the material's refractive index,  $n(\lambda)$ , and extinction coefficient,  $K(\lambda)$ , both taken at the illumination wavelength  $\lambda$ . The optical constants,  $n$  and  $K$ , vary with wavelength and are a function of the material's physical properties.

Equation 4.1 assumes a perfect "ideal" plane boundary between air and the material. It further assumes that the material is semi-infinite in thickness; that is, the

thickness of the material is large compared to the penetration of light into the material so that internal reflection does not need to be considered in computing the value of absolute reflectance.

High purity vacuum-evaporated planer film samples deposited on optically flat surfaces closely approximate the ideal conditions of equation 4.1(4). Similarly, single crystal highly polished and optically flat substrates also approximate the ideal condition. A microscope-based spectrophotometer using low power objective lenses and properly aligned optical illumination can illuminate a sample with light at nearly 90 degrees to the sample surface.

Measurement of the absolute reflectance of the sample material requires the use of a standard reference material. This permits aberrations present in the optical path to be nulled, because the aberration is seen equally by the sample and the reference and is cancelled out in the calculation of the relative reflectance.

The relative reflectance,  $R^*(\lambda)$ , is defined as the ratio of intensity of the light of wavelength  $\lambda$  reflected from the sample to the intensity of light at the same wavelength reflected from the reference material (4). The values of the reflected intensities must be corrected for background effects prior to calculation of the relative reference. This correction is done by the equipment automatically. The relative reflectance is given by equation 4.2 .

$$R^*(\lambda) = \frac{[\text{Intensity of reflected light from sample at } \lambda]}{[\text{Intensity of reflected light from reference at } \lambda]} \quad (4.2)$$

Modern spectrophotometers are designed to make measurements of the relative reflectance in a routine and straightforward manner as part of their normal operation.

#### 4.2.2 Calculating the Absolute Reflectance

Calculation of the absolute reflectance,  $R(\lambda)$ , of a sample material is a simple arithmetical operation when the relative reflectance,  $R^*(\lambda)$ , is available and the absolute reflectance,  $R_o(\lambda)$ , of the standard reference used to measure the relative reflectance is known. The computation is performed as follows (4):

$$R(\lambda) = R^*(\lambda) \times R_o(\lambda) \quad (4.3)$$

That is, the absolute reflectance of the sample at a certain wavelength  $\lambda$  is simply the product of the relative reflectance of the sample and the absolute reflectance of the reference at the same wavelength.

Conversely, the measured value of the relative reflectance,  $R^*(\lambda)$ , can be compared to tables of the theoretical value of  $R^*(\lambda)$  obtained using the theoretical values of absolute reflectance for the sample and reference material as determined by equation 4.1. The calculation of the theoretical relative reflectance for the sample is made as follows ( 4 ):

$$R^*(\lambda)_{Theor} = \frac{R(\lambda)}{R_o(\lambda)} \quad ( 4.4 )$$

#### 4.2.3 Experiment

##### a. Reflectance Measurements

The NaNospec/AFT Model 200 film thickness measurement system is a microscope-based spectrophotometer designed for measuring the reflectance of

materials commonly used in the processing of integrated circuit devices. The Model 200 measures the relative reflectance of sample materials at wavelengths between 370 and 800 nanometers (nm). The reflectance measurement is made on areas of 35 microns diameter, which permits the operator to examine small geometries in high density circuit devices in addition to the usual single layer planar films and substrates. A low power objective lens having a numerical aperture of 0.25 is used to illuminate the area of interest. A monochromator is employed to select the wavelength at which the reflectance value is to be measured.

The Nanospec/AFT allows the operator to obtain reflectance readings at one, two, or three wavelength settings selected by the operator, without the need to reset the instrument. Readings are reported in percent reflectance relative to the reference (equation 4.2). The Model 200 incorporates a statistical package which computes the average reflectance,  $R^*$ , standard deviation  $SR^*$  and minimum and maximum values of the reflectance  $R^*$ . The statistics are reported for each wavelength.

Single crystal silicon was chosen as standard reference. The silicon theoretical reflectance is shown in Table 4.1. Three wavelengths were chosen. 400 nm, 545 nm, 635 nm, which are close to the laser wavelength used in our measurements.

#### **b. Transmission Measurement**

Figure 4.2 shows the configuration of the transmission measurement. A 633 nm wavelength laser was chosen as the light source and the detector was a photodiode.

The laser intensity  $I_0$  was measured first. Then the sample was put vertically in the beam. The light passed through the metal film, and then struck the detector. This density is  $I_t$ .

The transmission is calculated as follows:

$$T = I_t/I_0$$

Table 4.1 Silicon Theoretical Reflectance (5)

$\lambda$ (nm)	R%
350	56.8
360	58.8
365	59.2
371	57.8
376	56.1
380	54.5
385	52.5
390	51.0
395	49.7
400	48.6
405	47.5
411	46.6
416	45.7
422	44.9
425	44.6
431	43.9
440	42.9
449	42.0
459	41.2
470	40.5
480	39.8
492	39.2
500	38.8
512	38.2
521	37.8
530	41.2
539	37.2
549	36.8
564	36.4
574	36.1
585	35.8
596	35.6
606	35.3
620	35.1
639	34.7
660	34.4

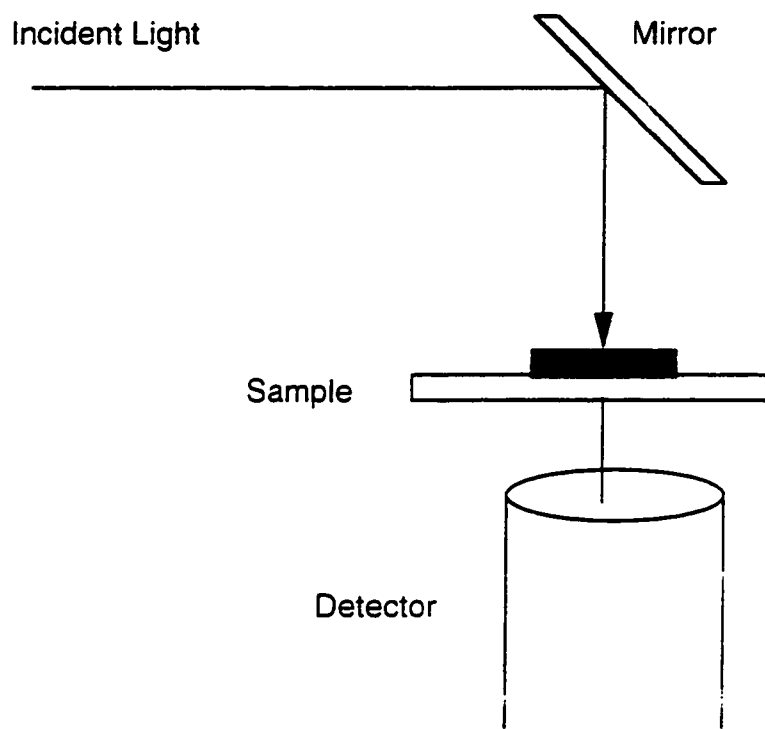


Figure 4.2 Transmission measurement system



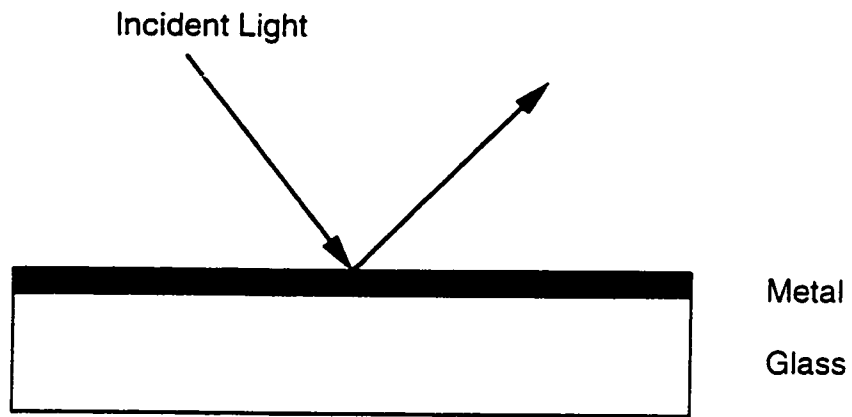
where  $T$  is the transmission.

### 4.3 Measurement of Mirror Material

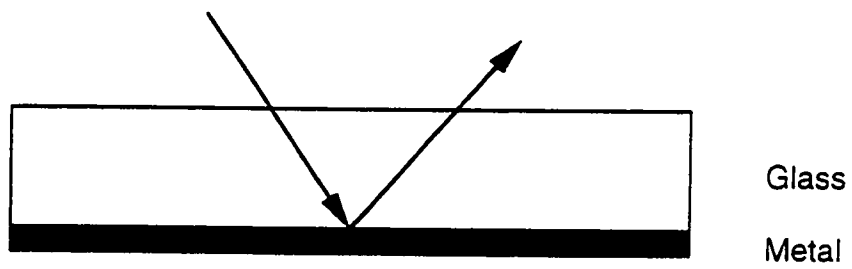
All metal-coated glass samples were obtained from the Alberta Microelectronic Centre (AMC). The metals were sputtered on the glass. Table 4.2 gives the absolute reflectance of the metal-coated glass samples. Column 3 is the reflectance of metal-air and column 4 is the reflectance of metal-glass. Figure 4.3 shows the schematic layout for the measurement. Because of the reflection and scattering of the glass, the column 2 data are lower than those of column 1.

Au, Ag, Cu, and Al have higher reflectance at 635 nm, which was used for our experiment. But Ag, Au, and Cu cannot be deposited on glass directly. To use these metals, a thin Cr film has to be deposited on the glass first. Then these metals are deposited on the Cr. Figure 4.3 shows the deposition and measurement.

Cr film exhibit low reflectivity. To decrease its affect, we tried to use thinner Cr film, and Au was chosen as the test metal. The thinnest Cr we could get is 133 Å. Table 4.3 shows the data for a 133 Å Cr film.



( a )



( b )

Figure 4.3 Reflectance measurement  
a ) Metal-air: b ) Metal-glass

Table 4.2 The Reflectivity of Some Metal Films

	Wavelength (nm)	Reflectivity (metal-air)	Reflectivity (metal-glass)
Al	400	94.62	83.01
	545	93.69	84.24
	635	93.10	83.94
Au	400	35.62	-----
	545	77.98	-----
	635	93.97	-----
Nb	400	42.28	40.92
	545	49.72	45.79
	635	52.78	48.37
Cu	400	33.39	-----
	545	55.57	-----
	635	93.83	-----
Cr	400	-----	37.76
	545	-----	40.15
	635	-----	41.71

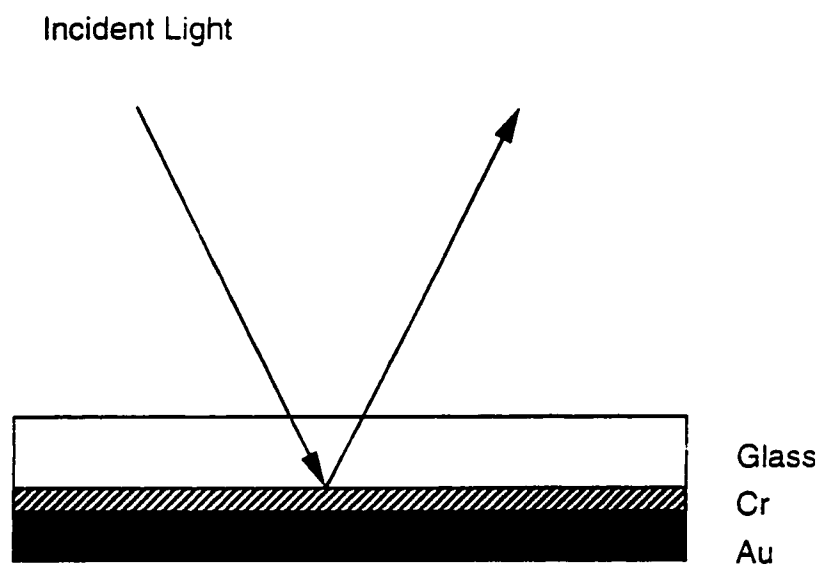


Figure 4.4 Thin Cr reflectance measurement of Au

Table 4.3 The Reflectivity of 133 Å Cr Covered with Au

	Wavelength(nm)	Reflectivity(%)
Cr	545	35.36
	635	41.33

From the data we obtained, we can see that even with 133 Å Cr film, the reflectivity is still as low as bulk Cr. Consequently, we used Al.

Al is highly reflective and easy to deposit on glass and easy to etch. However, it will be oxidized in air at high temperatures. For design 1, Al was deposited after bonding. However, in design 2, the first layer of metal had to be deposited before bonding. We were concern with the presence of the Al layer in terms of its effect on glass bonding. The Al may be oxidized and it may also affect the bonding. Consequently, some other tests, such as the effects of bonding, metal thickness and metal deposition, had to be done before we could use Al.

#### 4.4 The Bonding Effect Test

Al film 800 Å thick was sputtered on 200 μm thick 0211 glass. Then the Al was etched in concentrated HCl for 10 minutes. A 75 μm thick 0211 glass was used as cover glass to sandwich the Al between the glass. Both glasses were cleaned in a high pressure cleaner machine. These samples were bonded at 450 °C for 0.5 h. We then measured the reflectance and transmission. Table 4.5 is the comparison of

reflectance and transmission before and after bonding.

Because in design 2, the third piece of glass should be bonded on this sandwiched substrate in the same bonding condition, the 1 hour bonding test was done at 450 °C. The data are illustrated in Table 4.4.

**Table 4.4 The Effect of Bonding on Transmission and Reflectivity**  
The Thickness of Al is 800 Å

Deposition Method	Reflectivity (metal/glas)	Transparency		
		Before Bonding	0.5h Bonding	1.0h Bonding
Thermal-evaporation	84.3	0.044%	0.056%	0.080%
Al Sputter	88.6	0.00043%	0.00044%	0.044%

From the data, the bonding did not affect the reflectance too much, but it affected the transmission: in 1 hour bonding, the transmission changed 100-fold. Nevertheless, the absolute transmission was still low enough for our purpose.

#### 4.5 The Effect of Metal Film Thickness

In design 2, the metal was sandwiched between the glass plates. From our test a 2000 Å Al film could be bonded between the 75 µm and 200 µm 0211 glass plates. Thinner Al gave better bonding. The 600 Å, 800 Å, 1000 Å and 1500 Å Al films were tested, and reflectance and transmission were measured. Table 4.5

illustrates the data at different conditions.

**Table 4.5 The Effect of Thickness of Al Film on Transmission and Reflectivity**

Al thickness (Å)	Reflectivity (metal/glass)	Transmission	Bonding Quality
600	77.6%	0.63%	Excellent
800	85.6%	0.00043%	Excellent
1000	85.3%	0.00017%	Good
1500	85.2%	0.00011%	Good

From the data in Table 4.5, it is seen that 800 Å Al film yields similar reflectivity as thicker films, with similar transmission properties. In addition, the 800 Å Al showed the same bonding quality as 600 Å Al.

## **4.6 Deposition Method Effect**

The deposition method can affect the film properties in term of reflectance and transmission. Three deposition methods, thermal evaporation, and electrobeam evaporation sputter, were tested,. Table 4.6 illustrates the reflectance and transmission data with those different methods.

Of the methods used, sputtering yields films exhibiting the highest reflectivity and the lowest transparency.

**Table 4.6 Deposition Method of Al Affect on Transmission and Reflectivity**

Deposition method	Reflectivity ( metal/glass )	Transparency
Thermal Evaporation	84.3%	0.044%
Sputter	88.6%	0.00043%
Electrobeam Evaporation	86.7%	0.0080%

## 4.7 Summary

Aluminum proved to be the most effective metal mirror. Sputter deposition give the best reflection and transmission parameters. The 800 Å thick film has as low a transmission as thicker film, the same reflectivity and it gave the better bonding quality.

From above data, the metal parameters selected were 800 Å sputtering Al.



## References

1. OSA Handbook of Optics, McGraw-Hill, New York. 1978.
2. T. Gobmann; H. G. Schulz; D. Stover; H. P. Buchkremer; D. Jager. Proc. 3rd NTSC. *Thermal Spray Research and Applications*, Long Beach, CA. USA. 20-25 May, 1990, P. 503.
3. F. A. Jenkins,; H. E. White. Fundamentals of Optics, McGraw-Hill, New York. 1950.
4. Application Note No. 12-1. Nanometrics Inc. Sunnyvale, CA. 1988.
5. Handbook of Optical Constants of Solids, Academic Press. Orlando. 1985. Ed. Palik, E.D.;pp 397-399

## **Chapter Five: Chip Fabrication**

### **5.1 Introduction**

In multi-reflection cell fabrication, two major obstacles are the oxidation of Al and shrinkage of glass in the bonding stage. To avoid oxidation, the Al films are deposited and patterned after chip bonding. In the bonding stage, the substrate shrinks, making the alignment of the Al pattern mask difficult. To decrease this effect the lowest temperature and shortest bonding time were used. The details of the fabrication will be discussed in the following section.

### **5.2 The Fabrication of Design 1**

The flow channels were etched on 200  $\mu\text{m}$ -thick 0211 glass. Access holes were drilled into this etched substrate. The holes were drilled with carbide drills of diameter 0.145 inch (1). The drilled glass and 75  $\mu\text{m}$  glass, which would be used as cover glass, were cleaned. The 75  $\mu\text{m}$  cover glass was contacted with the substrate and then bonded at 450  $^{\circ}\text{C}$  for 0.5 h. The metal deposition and pattern steps are shown in Figure 5.1 and are described step by step as follows. All tapes we used are black tape in AMC.

a. The bonded pieces of chips were taped with black tape to cover the holes to prevent contamination of these holes from the solutions which would be used in the cleaning and etching steps. The tape was applied by hand. The other side of the chips were taped in the same place, because the alignment down the channel and at the corner of the chips would be used to align the metal mask, and we had to keep the alignment area unobstructed.

b. The remaining part of the chips was cleaned and deposited with 800  $\text{\AA}$  Al on

both sides. Photoresist was spun on the 200  $\mu\text{m}$  side.

c. Both tapes were peeled off. The alignment marks, which were at the corners and along the channels, could be seen and used to create the first side pattern. Then the lithography was done.

d. After the lithography was complete, the holes were taped as before to prevent them from being contaminated by solution in the developing and patterning steps. For the other side, the whole chip was taped to prevent the Al from being damaged in the pattern step.

e. The taped chips were developed and patterned.

f. After the first side was patterned, it was taped. The photoresist was spun on the other side and the first side tape was taken off.

g. To pattern the second side, the first side patterned alignment marks, which were along the channel and at the corner of the chip, were used for alignment to decrease the glass shrinkage effect on alignment. After alignment, the aperture pattern was moved 200  $\mu\text{m}$  down the channel. Lithography was then done.

h. The first side was taped to prevent the patterned Al on the first side from being damaged in the etching steps, and then the Al was patterned.

i. After the second side was patterned, the tape was taken off and the fabrication was finished.

Figure 5.1 shows the complete steps of the first design fabrication.

### **5.3 The Fabrication of Design 2**

In design 2 fabrication we met some new problems: after the first layer of Al was patterned, the Al had to be sandwiched between the glass. The glass with patterned Al had to be cleaned. We always use  $\text{H}_2\text{SO}_4:\text{H}_2\text{O}_2=3:1$  or  $\text{NH}_3:\text{H}_2\text{O}_2=3:1$  to clean the glass. But these solutions would damage the Al film, so a new cleaning program had to be used for this cleaning. A second problem was the three piece bonding, which has been described in Chapter 4. The third problem was that the access holes had to be drilled on the bonded piece, because we cannot drill holes on

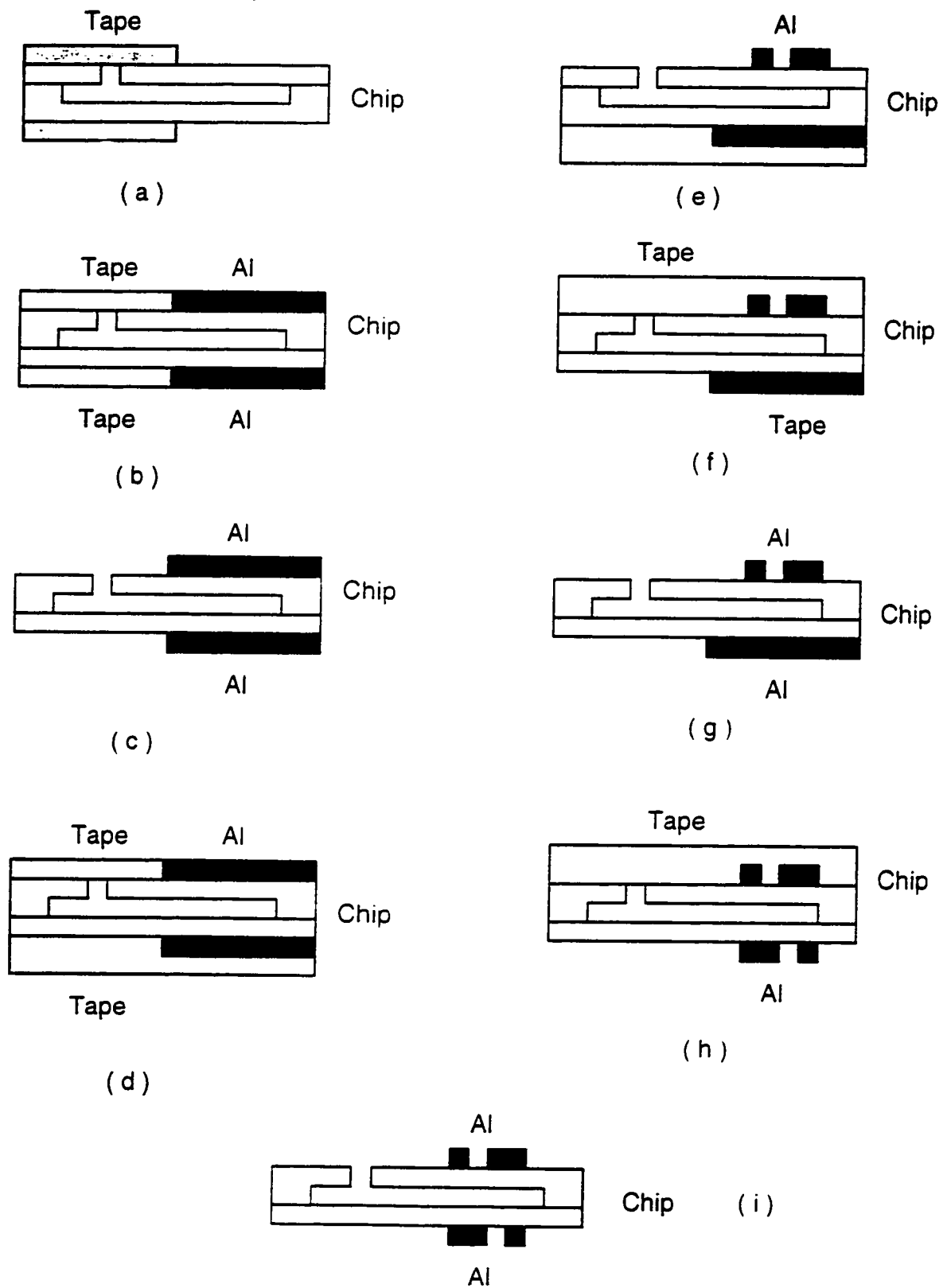


Figure 5.1 Fabrication procedure of design 1

75  $\mu\text{m}$  glass. Some tests had to be done first.

### 5.3.1 The Test of Al Coated Glass Cleaning

For blank glass cleaning, the normal method is to use  $\text{H}_2\text{SO}_4:\text{H}_2\text{O}_2=3:1$  or  $\text{NH}_3:\text{H}_2\text{O}_2=3:1$  (2). In these solutions, the  $\text{H}_2\text{SO}_4$  is used to oxidize the organic contamination on the glass, whereas  $\text{NH}_3$  wets the glass well, so the dirt on the glass surface is dissolved. If the glass has Al on it, these solutions can not be used.  $\text{H}_2\text{SO}_4$  dissolves the Al to  $\text{Al}_2(\text{SO}_4)_3$ , while  $\text{H}_2\text{O}_2$  oxidizes the Al, and the oxidized Al reacts with  $\text{NH}_3$  to form  $\text{Al}(\text{NH}_3)_6^{3+}$ . Either process damages the Al.

To clean the glass, some organic solvent, such as methanol, alcohol, acetone, etc., were tested. However, the impurities remained on the substrate, and the glass could not be bonded. We had to try some new programs for this cleaning.

Al will be passivated in concentrated  $\text{HNO}_3$  (3).  $\text{HNO}_3$  can oxidize organic impurities much like  $\text{H}_2\text{SO}_4$  does. The glass with Al on it was put in concentrated  $\text{HNO}_3$  for half an hour and then the reflection and transmission were tested. Reflection was done through glass. Table 5.1 illustrates the data after washing.  $\text{HNO}_3$  did not damage the Al significantly. But before the  $\text{HNO}_3$  was used, acetone was used to remove the photoresist that remained on the glass as a result of the Al patterning step. Methanol was used to clean the acetone residue. The whole cleaning steps were as follows: Acetone, 30 min; Methanol, rinse;  $\text{HNO}_3$ , 30 min Distill water, rinse.

Table 5.1 The Effect of  $\text{HNO}_3$  on Transmission and Reflectance of Al Film

	Reflectance ( 633 nm )	Transmission ( 633 nm )
Before $\text{HNO}_3$ washing	88.6%	0.00043%
After $\text{HNO}_3$ washing	86.7%	0.00057%

This cleaned glass was washed with high pressure water and then contacted and bonded. With this new cleaning program, we obtained the same bonding quality as with the other program for the blank glass bonding.

### **5.3.2 Drilling Test on Bonded Glass**

An 800 Å thick Al film was sputter deposited on 500 µm thick 0211 glass, patterned, and then cleaned using the program described in Section 6.3.1. Another 75 µm glass was cleaned with pirhana. Both the substrate and 75 µm glass were cleaned with high pressure water, contacted and bonded at 450 °C for half an hour. Holes were drilled on this bonded piece, and all test pieces survived. The quality of the holes were the same as that of the normal glass, meaning that we could drill the holes in the bonded glass using the same method as for normal glass.

### **5.3.3 The Fabrication of Design 2**

Figure 5.2 illustrates the entire fabrication process. What follows is a detailed explanation of Figure 5.2.

a. The 200 µm- or 500 µm-thick glass, used as a handle wafer, was sputter deposited with 800 Å Al film. This Al film was patterned with the same mask that used in design 1.

b. This patterned glass was cleaned with the program described in section 5.3.1. Another piece of 75 µm glass was cleaned with  $\text{H}_2\text{SO}_4:\text{H}_2\text{O}_2=3:1$  and rinsed with water. Both the handle wafer and the 75 µm glass were cleaned with the high pressure rinser, and then contacted. The patterned Al was sandwiched between the glass, and the contacted glass was bonded at 450 °C for 0.5 h.

c. A channel was etched on this bonded piece on the 75 µm glass side and then access holes were drilled in it.

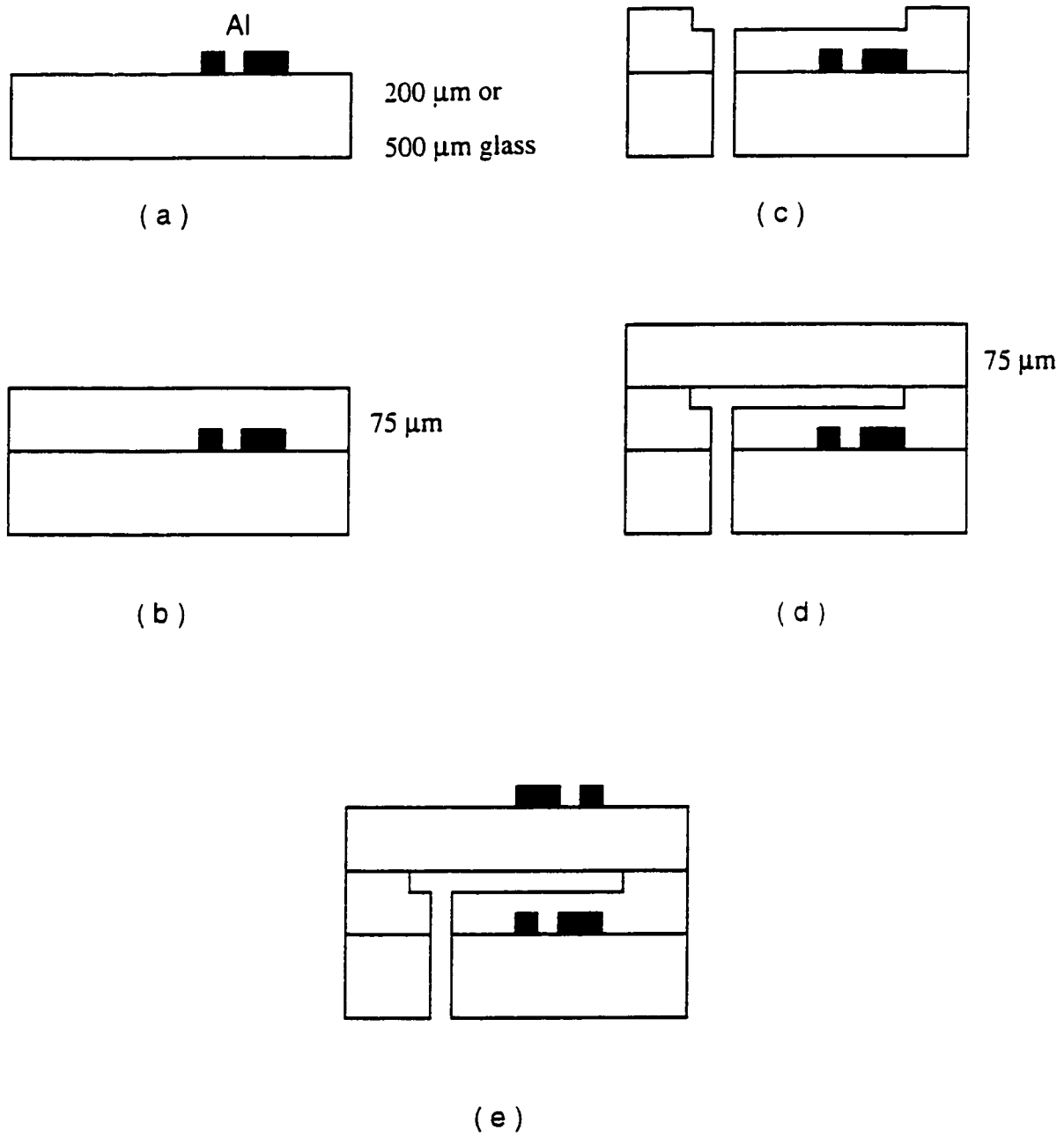


Figure 5.2 Fabrication procedure of design 2

d. The chip was washed with acetone and then  $\text{H}_2\text{SO}_4:\text{H}_2\text{O}_2=3:1$  for 0.5 h. The 75  $\mu\text{m}$  glass was cleaned in the same way. Then both were cleaned with high pressure water, contacted, and then bonded at 450  $^\circ\text{C}$  for 0.5 h.

e. Half of this bonded chip was taped on the cover piece side. Another half was cleaned and deposited with 800  $\text{\AA}$  Al film. Then the tape was taken off. For this Al pattern, the patterned alignment on the first Al layer was used to align the mask. After the lithography was done, the holes were taped to prevent them from being contaminated by the developing and etching solutions.

## 5.4 Conclusion and Discussion

Because of the short detection plug and short separation distance in microchip-based capillary electrophoresis, fabrication of the absorption cell is a major challenge. Theoretically, a thinner glass substrate can provide better sensitivity in a multiple reflection absorption cell. But it is difficult to fabricate. Design 2 proved that a 75-75  $\mu\text{m}$  glass substrate can be achieved by using a thicker handle wafer glass. Drilling on bonded glass and three piece glass bonding may be useful in other fabrications.

By using this handle wafer design, the glass can be polished before channel etching and after the channel is covered. This means that other thinner chips can be achieved, improving the sensitivity.

This design includes more fabrication steps than in normal chip fabrication, but compared with the U-cell design, it avoids having to insert optical fibers.

## References

1. Laboratory Manual in D.J. Harrison Group, Chem. Depart. Univ. of Alberta.
2. Fan, Z. H.; Harrison, D. J. *Anal. Chem.* 1994, 66, 177-184.
3. *Comprehensive Inorganic Chemistry*, J. C. Bailar, Vol. 1 pp 1002.



## **Chapter Six: Measurements, Results and Discussion**

### **6.1 Introduction**

Two basic problems for a microfabricated multi-reflection absorption cell are the design of the cell and the setup of the detection system or measurement equipment. The absorption cell should be easy to manufacture and have high sensitivity. The detection system must be convenient to use. In IR-spectroscopy, detection cells are available. For this microchip-based multi-reflection absorption cell, the angle of incident light should be changable since the light throughput angle must be adjusted to achieve high light throughput. This requires that the position of the chip and detector must be changable.

### **6.2 Instrumentation**

The optical instrumentation setup is illustrated in Figure (6.1). A 2 mW, 633 nm He-Ne laser was used as a source. A mirror mounted on rotary and Z-translation stages was used to control the height above the aperture and the incident angle to  $\pm 0.02$  degree precision. The absolute angle relative to the surface was determined to within  $\pm 0.02$  degrees by replacing a chip with a mirror and adjusting the angle to superimpose the incident beam on the reflected beam. Light was detected through the exit aperture with a photodiode (either 10 or 31 mm area, Melles Griot) mounted on an x-y translation stage, amplified with a wide dynamic range current amplifier (Model 13AMP003, Melles Griot) and recorded with a National Instruments (Austin, TX) Lab PC- plus A/D converter and a Pentium 90 Mhz personal computer. Data were acquired at 50 kHz, and 5000 points were averaged in

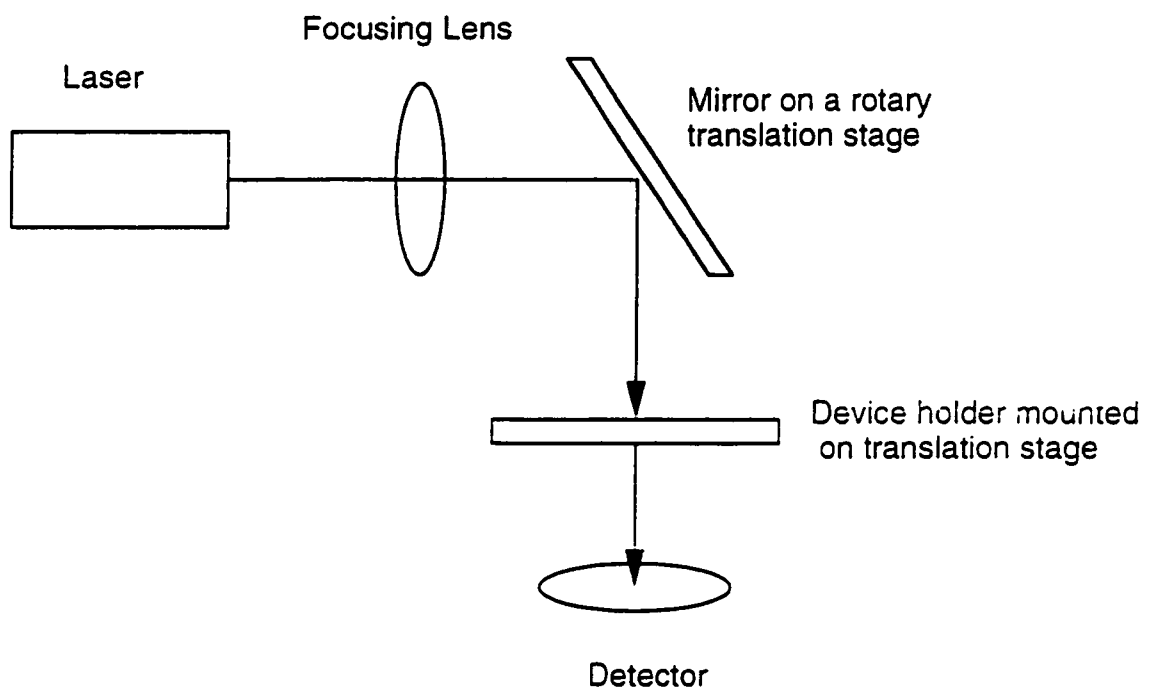


Figure 6.1 The optical instrumentation setup

real time to write data at a net rate of 10 Hz. Software was written in Labview (National Instruments). As previously described (2), a computer-controlled power supply and relay unit were used for potential control of the chip device.

### **6.3 Reagents**

Bromothymolblue (BTB) (BDH Chemicals, Toronto, ON) was prepared in 5 mM, pH 10.5 phosphate buffer in concentrations between 5 and 500  $\mu\text{M}$ . The absorbtivity coefficient of 10  $\mu\text{M}$  BTB was measured with an HP diode array spectrometer to be  $3.27 \times 10^4 \text{ M/cm}^{-1}$  at 633 nm in the same buffer. In either case, the sample buffer was used as the CE running buffer. To avoid sample stacking effects. Solutions were filtered through a 0.22  $\mu\text{m}$  pore syringe filter (Nylon, Chromatographic Specialties, Brokeville, ON) before being introduced into the chips.

### **6.4 Procedures**

Sample injections were performed with 1 kV applied for 10s between the sample and sample waste reservoir. This gave a geometrically-defined sample plug at the double-T injection created by the offset between the sample and sample waste channel (3,4,5). Separation was performed with 6 kV across the 6.78 cm channel between the buffer and waste reservoirs.

### **6.5 Light Throughput and Noise**

The angle of incidence and thus, the number of reflections affects the light throughput in the multi-reflection cell because light intensity as a result of scattering and transmission at the surface of the glass and metal (6,7). The path length change

will affect the scattering of light in the sample and glass. Studies were performed in order to determine usable angles of incidence. Figure 6.2 shows the setup of the experiment. Two mirrors were pressed together. The mirrors overlapped by 200  $\mu\text{m}$ . A laser and a diode detector were used and incident beam angles were varied. Figure 6.3 shows the transmission intensity versus incident angle indicating the concept.

For a real chip only certain angles can give high light throughput. Figure 6.4 shows the light throughput change with the incident light angle, as measured by Dr. H. Salimi-moosavi (8). Design 1 gives three higher light throughput angles at about 3, 4 and 5.5 degree. Design 2 gives more complicated maxima in the range of 2--8 degrees.

To evaluate the throughput of the multi-reflection design, comparison was made to a "single pass" device fabricated with a 10  $\mu\text{m}$  depth and no offset between the entrance and exit apertures. Figure 6.5 shows the device. Light at 0 degree incidence passed straight through, undergoing no reflections and giving a detector response of 13.00  $\mu\text{A}$  as measured by H. Salimi-moosavi (8). Figure 6.4 shows that the typical diode currents at the angle maxima were 10 to 100-fold lower than those for the single pass device. The loss in intensity with decreasing angle in Figure 6.4 is expected with the increasing number of reflection and divergence of the beam. The lack of intensity below about  $2.5^\circ$  is ascribed to the reflection of most of the beam back out of the 30  $\mu\text{m}$  entrance aperture.

## 6.6 Sensitivity

Because absorbance is the ratio of intensities,  $\log I/I_0$ , the measurement is not directly affected by the losses incurred while the beam transits the cell. The signal-to-noise ratio decreases as the transmitted intensity drops. The detection limit is affected by the intensity of the transmission. The sensitivity should be increased by

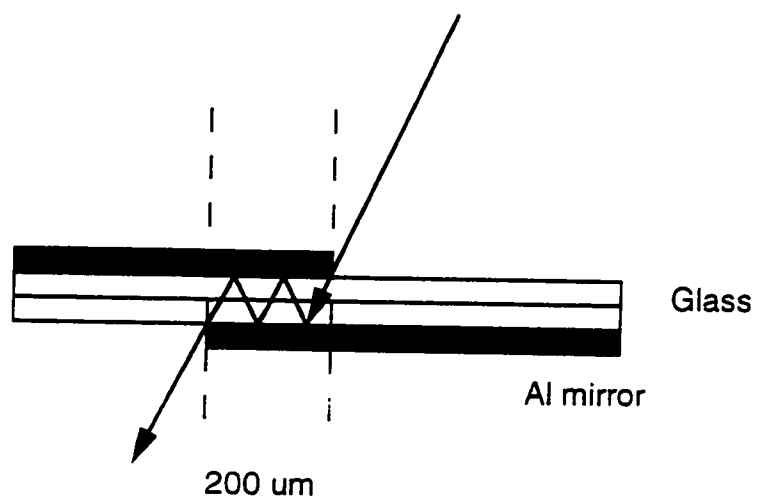


Figure 6.2 The initial mirror test setup to show the multiple reflection cell could work

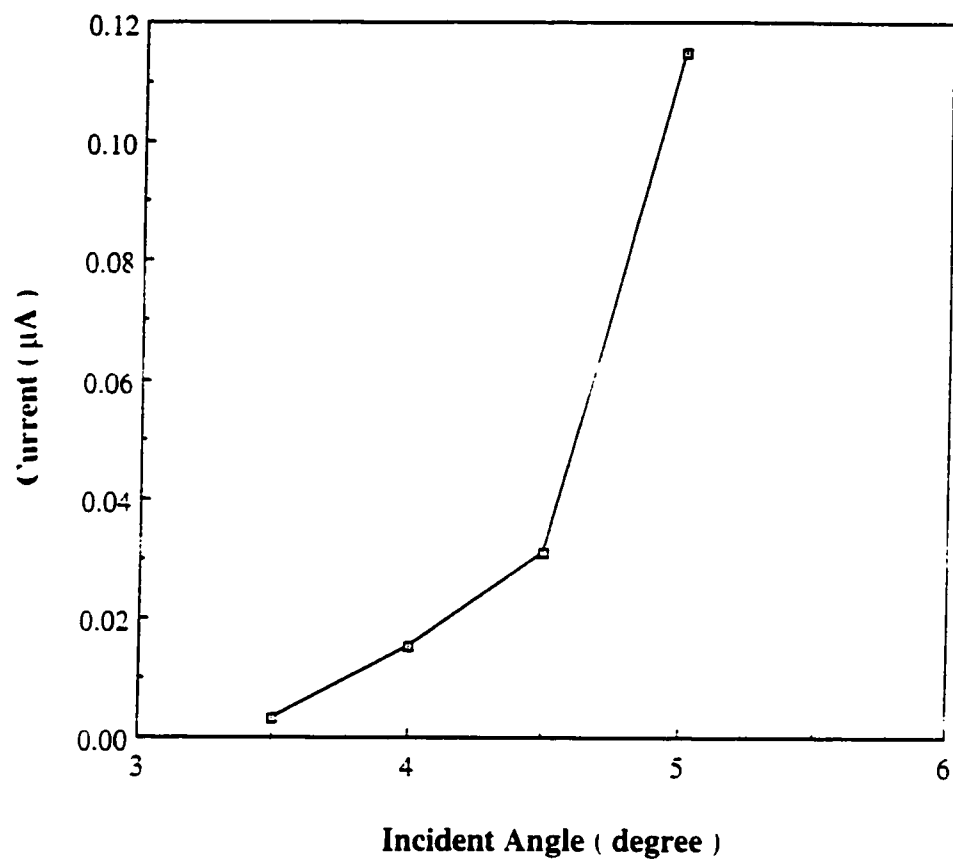


Figure 6.3 Intensity versus incident beam angle of plain mirror

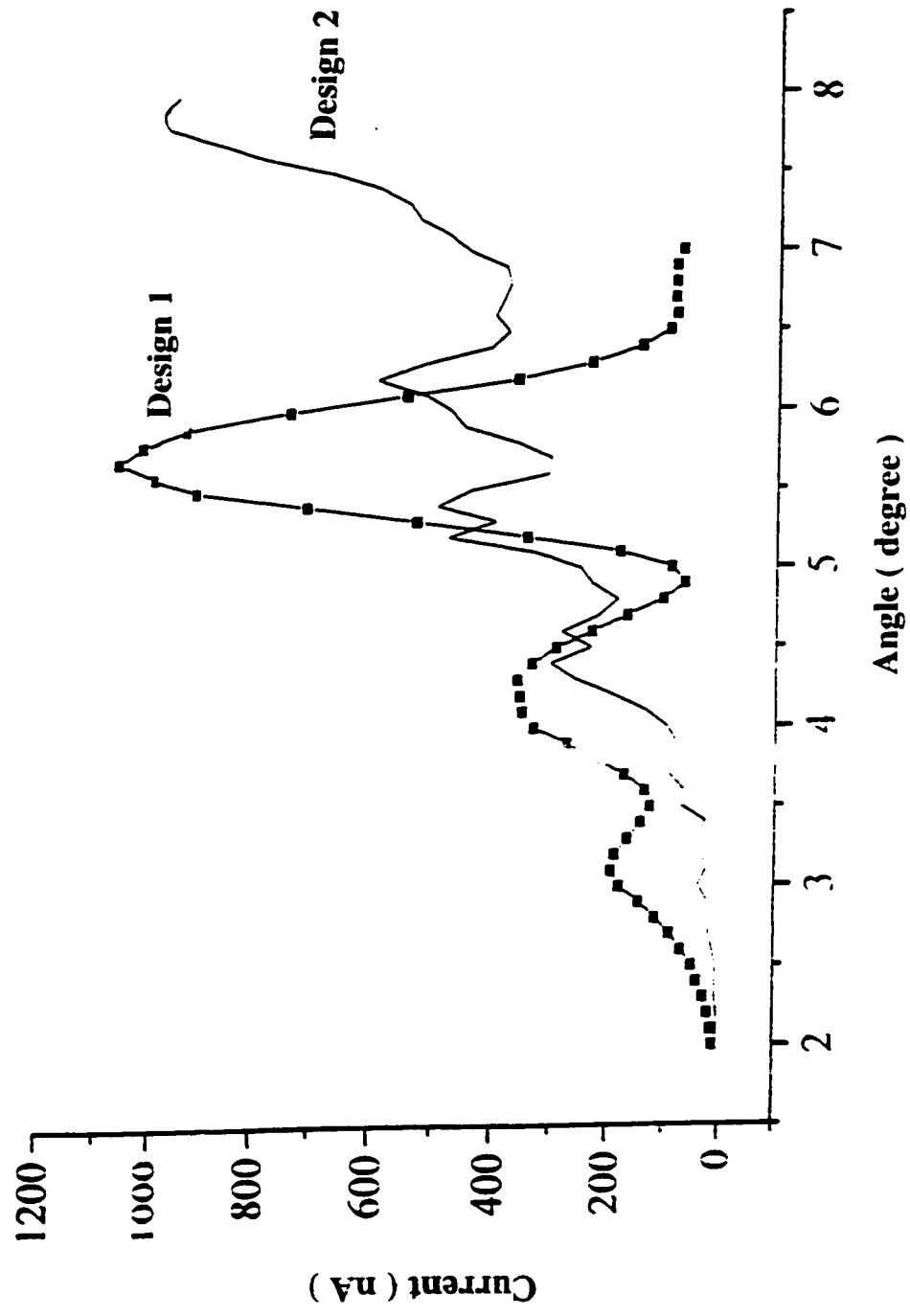


Figure 6.4 Diode photocurrent as a function of incident beam angle(8)

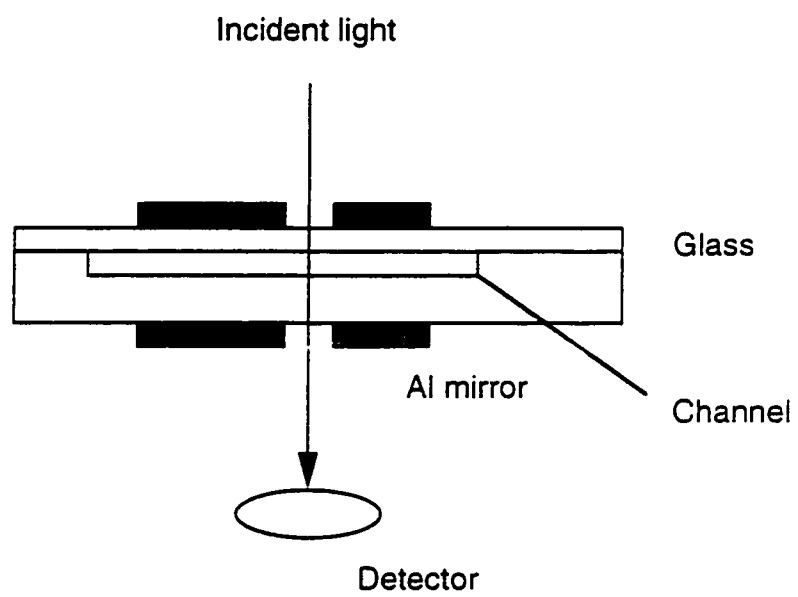


Figure 6.5 No offset device



increasing the path length through solution, but the enhancement may not be as large as expected. For example, a fused silica capillary-based multi-reflection cell described by Wang *et al.*(9) gave an experimental sensitivity corresponding to path length of 1 mm. For this reason, we calculated the effective path length,  $L$ , which was determined from the slopes of measured calibration curves for each device.

Figure 6.6 shows the effective path length as a function of incident angle for all of the etch depths and device designs as measured by H. Salimi-moosavi (8). Increasing the depth of the channel gives longer path length. Comparing design 1 and design 2, the thinner glass substrate gives larger path length and high sensitivity. The lowest detectable concentration of design 1 is  $10^{-4}$  M for a 10  $\mu\text{m}$ -deep channel. For design 2,  $10^{-5}$  M has been detected with a signal-to-noise ratio of 63. Figure 6.7 shows the peak of  $10^{-5}$  M solution. Because the detection limit is signal-to-noise ratio of 3, lower concentration should be detectable. But I did not get that in my experiment. This is because the noise of the light source. Lower concentration can be detected by improving the light source or adding an electronic filter to reduce the noise.

## 6.7 Calibration Curve

Figure 6.8 shows the calibration curve of design 2. The incident angle was  $6^\circ$ . It is approximately linear in the range of 10  $\mu\text{M}$  to 1000  $\mu\text{M}$ .

## 6.8 Result and Discussion

The expected increase in path length can be calculated, and a comparison of Figure 2.3 a) and Figure 6.5 shows that effective path length is about 40-50 % of the calculated path length in most cases. A greater discrepancy of 28-40 % was seen for the design 2 device at angles of about 3-6 degrees. We have not identified the

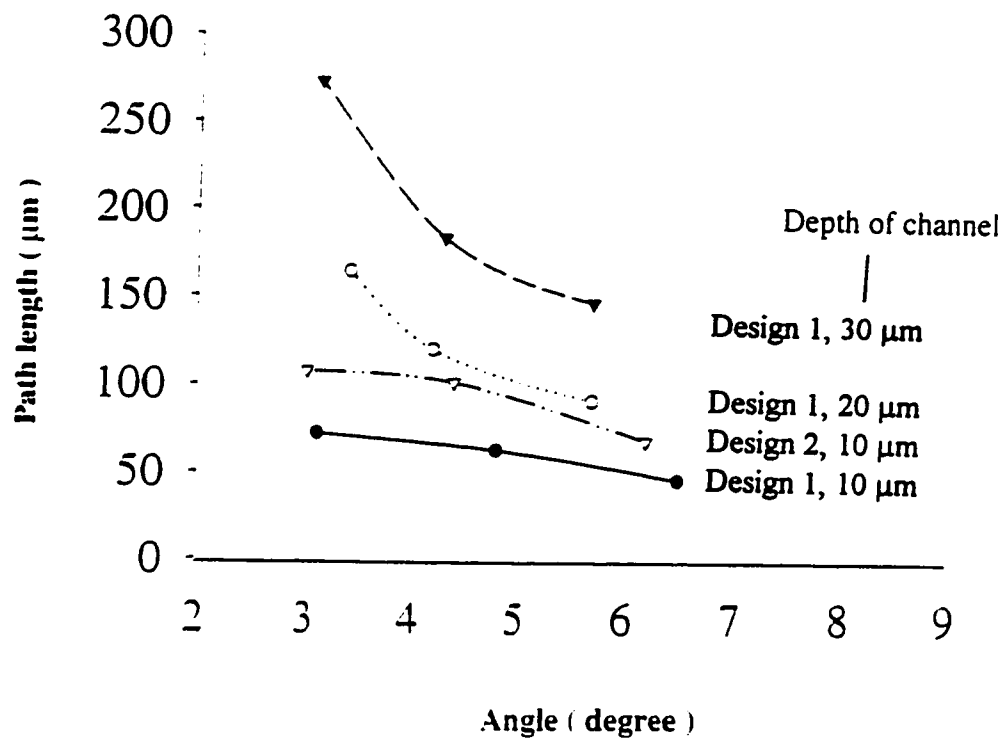


Figure 6.6 Effective path length as a function of incident beam(8)

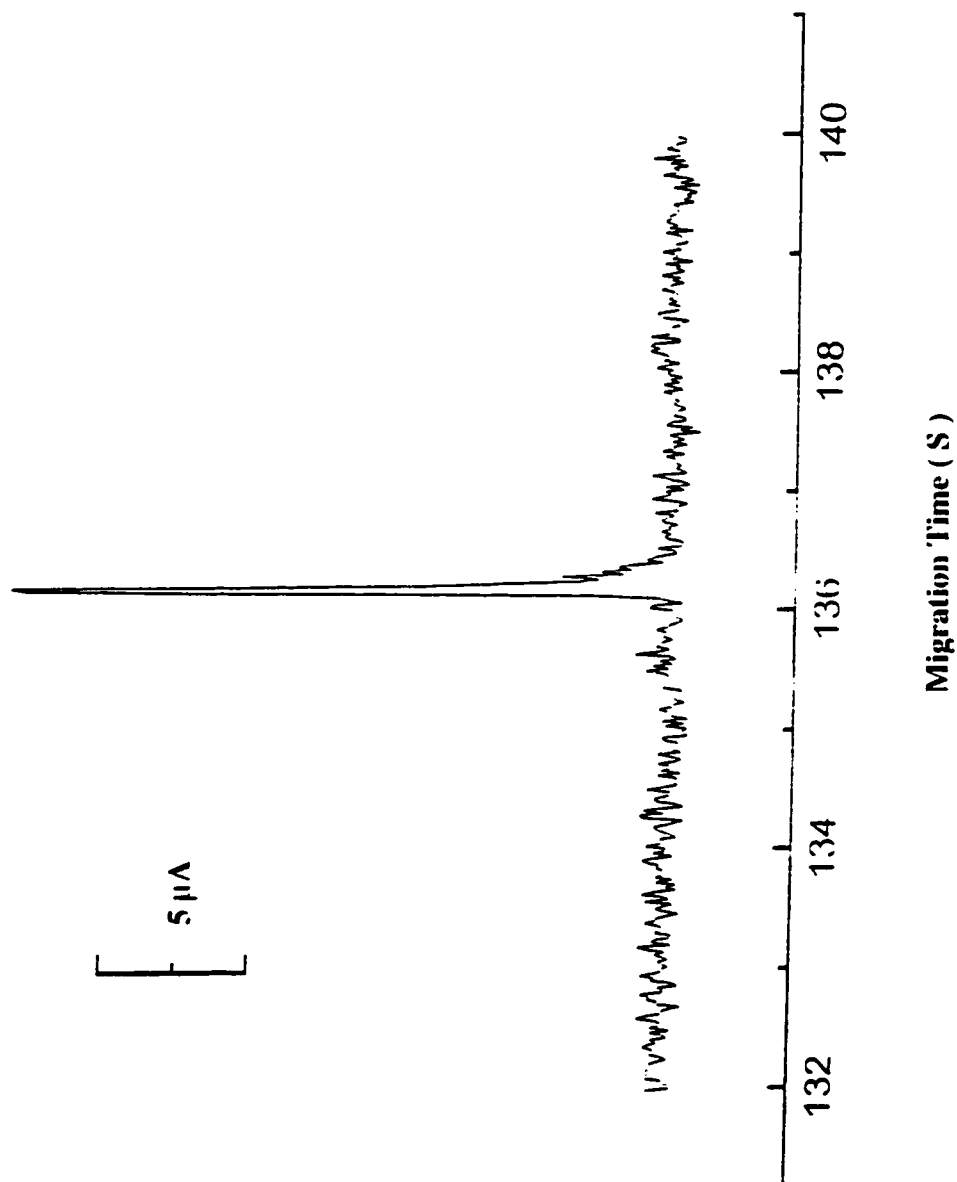


Figure 6.7  $10^{-5}$  M BTB absorbance peak

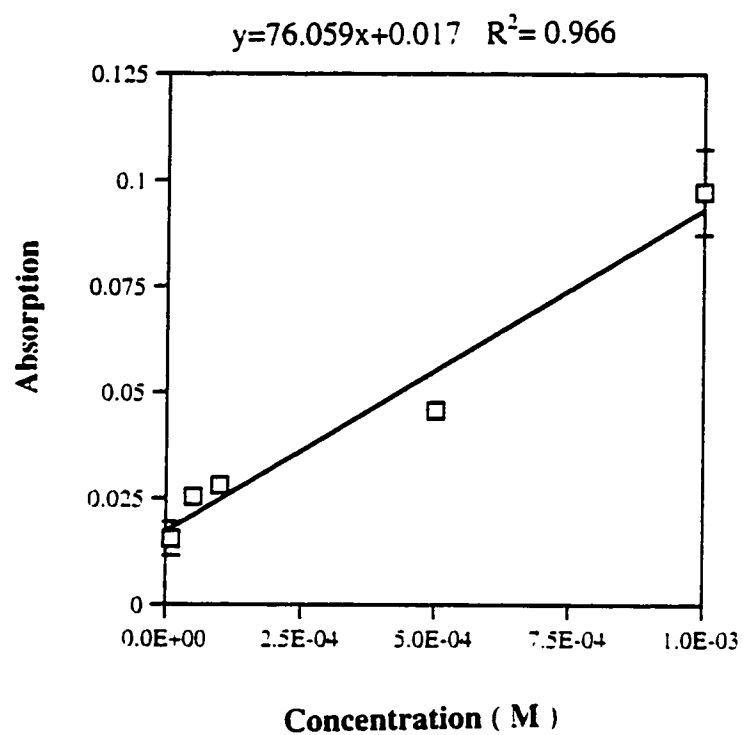


Figure 6.8 BTB calibration curve of design 2

source of this discrepancy, but do note that such effects have been observed by others for multi-reflection cells(8). Possible causes include the use of single ray trace model to describe the beam path, rather than a more complete treatment of the device as an etalon-type waveguide. Calculations indicate that 10% variations from the nominal values in glass thickness, etch depth, inter-aperture separation distance, or accuracy of the incident light angle each amount to no more than a 10 % error. Since these experimental errors are unlikely to all combine in one direction, or to be the same between all devices, the discrepancy is not fully explained. Nevertheless, the data in Figure 6.6 confirm that the sensitivity is increased 5-10 fold by the use of a multi-reflection cell, compared to a straight-pass design for a device of the same etch depth. Comparison of the sensitivity of designs 1 and 2 confirms that decreasing the thickness of the glass through which the light travels is beneficial to sensitivity, although at the expense of greater fabrication complexity.

The detector volume contributes to the band broadening of a peak. The inter-aperture distance of 200  $\mu\text{m}$  was selected to minimize the dispersion contributed by the detector, while still allowing for large numbers of reflections. A measurement of the separation efficiency was made using fluorescence detection of fluorescein excited at 488 nm as the standard, since a detector window length along the channel of 30-40  $\mu\text{m}$  was easily achieved with a focused beam. The results were complicated by the concentration dependent band broadening we observed for both fluorescein and BTB, which apparently arises from surface adsorption. A 9 kV separation voltage gave 108,000 theoretical plates for 10 nM fluorescein, 66,000 plates at 100 nM and 8000 plates at 1  $\mu\text{M}$ . A 10  $\mu\text{M}$  deep multi-reflection absorbance cell gave  $8,000 \pm 2,000$  plates for  $< 100 \mu\text{M}$  BTB, declining to  $3,500 \pm 1,100$  plates at 500  $\mu\text{M}$  and  $1,800 \pm 200$  plates at 1 mM. We attribute these concentration-dependent efficiencies to surface adsorption effects, although sample overloading may contribute at the highest concentrations. The results indicate that at similar concentrations of these dyes both the fluorescence detector and the absorbance cell give similar efficiencies. Another test of the effect of the adsorption

cell was made using the single pass device, which should have an approximate detector window length of 30-40  $\mu\text{m}$ , given the 30  $\mu\text{m}$  apertures in the mirrors. At 1 mM we observed  $1,800 \pm 1,300$  plates and at 500  $\mu\text{M}$ ,  $4,300 \pm 2,200$  plates, which is in agreement with data for the 10  $\mu\text{m}$ -deep multi-reflection cell. We conclude that the inter-aperture distance doesn't make a significant contribution to band broadening of the BTB sample.

## 6.9 Conclusions

Absorbance detection is a very important tool in CE, but the poor path lengths achieved within microchip devices are a serious detriment to its use. Previous work on microfabricated absorbance cells has produced devices made in silicon, which are not well suited to CE applications due to the use of high electric fields, or glass devices which would not be well suited to mass microfabrication. The device presented here is a significant step forward in developing a realistically useful microchip absorbance cell, which extends the range of samples that can be analyzed by microchip CE. In fact, these devices could be coupled to a capillary and serve as a detector cell as a component of a larger unit. While the work was demonstrated with a laser source it certainly will work with other white light sources. In addition, the transition from visible to the ultra-violet will be readily accomplished by combining the methods presented here with established methods to micromachine Quartz devices.

## Reference

1. Liang, Z.; Chiem, N.; Gevirk, G.; Tang, T.; Fluri, K.; Harrison, D. J. *Anal. Chem.* 1996, 68, 1040-1046.
2. Seiler, K.; Harrison, D. J.; Manz, A. *Anal. Chem.* 1993, 65, 2637-2642.
3. Salimi-Moosavi, H.; Tang, T.; Harrison, D. J. *J. Am. Chem. Soc.* 1997, 119, 8716-8717.
4. Chiem, N.; Harrison, D. J. *Anal. Chem.* 1997, 69, 373-378.
5. Effenhauser, C. S.; Manz, A.; Widmer, H. M. *Anal. Chem.* 1993, 65, 2637-2641.
6. Stephens, E. R. *Appl. Spectrosc.* 1958, 13, 80-84.
7. Werle, P.; Slemr, F. *Appl. Opt.* 1991, 30, 430-434.
8. H. Salimi-moosavi, University of Alberta, 1998, private communication.
9. Wang, T.; Aiken, J. H.; Huie, C. W.; Hartwick, R. A. *Anal. Chem.* 1991, 63, 1372-1376.